

1 A channel selection method for hyperspectral  
2 atmospheric infrared sounders based on  
3 layering

4 Shujie Chang<sup>1,2,3</sup>, Zheng Sheng<sup>1,2</sup>, Huadong Du<sup>1,2</sup>, Wei Ge<sup>1,2</sup> and  
5 Wei Zhang<sup>1,2</sup>

6 <sup>1</sup> College of Meteorology and Oceanography, National University of  
7 Defense Technology, Nanjing, China

8 <sup>2</sup> Collaborative Innovation Center on Forecast and Evaluation of  
9 Meteorological Disasters, Nanjing University of Information  
10 Science and Technology, Nanjing, China

11 <sup>3</sup> South China Sea Institute for Marine Meteorology, Guangdong  
12 Ocean University, Zhanjiang, China

13

14 **Correspondence:** Zheng Sheng (19994035@sina.com)

15

16 **Abstract.** Because a satellite channel's ability to resolve  
17 hyperspectral data varies with height, an improved channel selection  
18 method is proposed based on information content. An effective  
19 channel selection scheme for a hyperspectral atmospheric infrared  
20 sounder using AIRS data based on layering is proposed. The results  
21 are as follows: (1) Using the improved method, the atmospheric  
22 retrievable index is more stable, the value reaching 0.54. The

23 coverage of the weighting functions is more evenly distributed over  
24 height with this method and closer to the actual atmosphere; (2)  
25 Statistical inversion comparison experiments show that the accuracy  
26 of the retrieval temperature, using the improved channel selection  
27 method in this paper, is consistent with that of 1Dvar channel  
28 selection. In the stratosphere and mesosphere especially, from 10 hPa  
29 to 0.02 hPa, the accuracy of the retrieval temperature of our  
30 improved channel selection method is improved by about 1 K. In  
31 general, the accuracy of the retrieval temperature of ICS (Improved  
32 Channel Selection) is improved; (3) Statistical inversion comparison  
33 experiments in four typical regions indicate that ICS in this paper is  
34 significantly better than NCS (NWP Channel Selection) and PCS  
35 (Primary Channel Selection) in different regions and shows  
36 latitudinal variations, which shows potential for future applications.

37

## 38 **1 Introduction**

39 Since the successful launch of the first meteorological satellite,  
40 TIROS in the 1960s, satellite observation technology has developed  
41 rapidly. Meteorological satellites observe the Earth's atmosphere  
42 from space and are able to record data from regions which are  
43 otherwise difficult to observe. Satellite data greatly enrich the  
44 content and range of meteorological observations, and consequently,

45 atmospheric exploration technology and meteorological observations  
46 have taken us to a new stage in our understanding of weather  
47 systems and related phenomena (Fang, 2014). From the perspective  
48 of vertical atmospheric observation, satellite instruments are  
49 developing rapidly. In their infancy, the traditional infrared  
50 measurement instruments for detecting atmospheric temperature and  
51 moisture profiles, such as TOVS (Smith et al., 1991) or HIRS in  
52 ATOVS (Chahine, 1972; Li et al., 2000; Liu, 2007), usually  
53 employed filter spectrometry. Even though such instruments have  
54 played an important role in improving weather prediction, it is  
55 difficult to continue to build upon improvements in terms of  
56 observation accuracy and vertical resolution due to the limitation of  
57 low spectral resolution. By using this kind of filter-based  
58 spectroscopic measurement instrument, therefore, it is difficult to  
59 meet today's needs in numerical weather prediction (Eyre et al.,  
60 1993; Prunet et al., 2010; Menzel et al., 2018). To meet this  
61 challenge, a series of plans for the creation of high-spectral  
62 resolution atmospheric measurement instruments has been executed  
63 in the United States and in Europe in recent years: One example is  
64 the AIRS (Atmospheric InfraRed Sounder) on the Earth Observation  
65 System, "Aqua", launched on May 4, 2002 from the United States.  
66 AIRS has 2378 spectral channels providing sensitivity from the

67 ground to up to about 65 km of altitude (Aumann et al., 2003;  
68 Hoffmann and Alexander, 2009; Gong et al., 2011). The United  
69 States and Europe, in 2010 and in 2007, also installed the CRIS  
70 (Cross-track Infrared Sounder) and the IASI (Inter-Attractive  
71 Atmospheric Sounding Interferometer) on polar-orbiting satellites.

72 China also devotes great importance to the development of such  
73 advanced sounding technologies. In the early 1990s, the National  
74 Satellite Meteorological Center began to investigate the principles  
75 and techniques of hyperspectral resolution atmospheric observations.  
76 China's development of interferometric atmospheric vertical  
77 detectors eventually led to the launch of Fengyun No. 3, on May 27,  
78 2008, and Fengyun No. 4 on December 11, 2016, both of which  
79 were equipped with infrared atmospheric instruments. How best to  
80 use the hyperspectral resolution observation data obtained from  
81 these instruments, to obtain reliable atmospheric temperature and  
82 humidity profiles, is an active area of study in atmospheric inversion  
83 theory.

84 Due to technical limitations, only a limited number of channels  
85 could at first be built into the typical satellite instruments. In this  
86 case, channel selection generally involved controlling the channel  
87 weighting function by utilizing the spectral response characteristics  
88 of the channel (such as center frequency and bandwidth). With the

89 development of measurement technology, increasing numbers of  
90 hyperspectral detectors were carried on meteorological satellites.  
91 Due to the large number of channels and data supported by such  
92 instruments today (such as AIRS with 2378 channels and IASI with  
93 8461 channels), it has proven extremely cumbersome to store,  
94 transmit, and process such data. Moreover, there is often a close  
95 correlation between the channels, causing an ill-posedness of the  
96 inversion, potentially compromising accuracy of the retrieval  
97 product based on hyperspectral resolution data.

98 However, hyperspectral detectors have many channels and  
99 provide real-time mode prediction systems with vast quantities of  
100 data, which can significantly improve prediction accuracy. But, if all  
101 the channels are used to retrieve data, the retrieval time considerably  
102 increases. Even more problematic are the glut of information  
103 produced, and the unsuitability of the calculations for real-time  
104 forecasting. Concurrently, the computer processing power must be  
105 large enough to meet the demands of simulating all the channels  
106 simultaneously within the forecast time. It is important to properly  
107 select a group of channels that can provide as much information as  
108 possible from the thousands of channels' observations to improve the  
109 calculation efficiency and retrieval quality.

110 Many researchers have studied the channel selection algorithm.

111 Menke (1984) first chose channels using a data precision matrix  
112 method. Aires et al. (1999) made the selection using the Jacobian  
113 matrix, which has been widely used since then (Aires et al., 2002;  
114 Rabier et al., 2010). Rodgers (2000) indicated that there are two  
115 useful quantities in measuring the information provided by the  
116 observation data: Shannon information content and degrees of  
117 freedom. The concept of information capacity then became widely  
118 used in satellite channel selection. In 2007, Xu (2007) compared the  
119 Shannon information content with the relative entropy, analyzing the  
120 information loss and information redundancy. In 2008, Du et al.  
121 (2008) introduced the concept of the atmospheric retrievable index  
122 (ARI) as a criterion for channel selection, and in 2010, Wakita et al.  
123 (2010) produced a scheme for calculating the information content of  
124 the various atmospheric parameters in remote sensing using  
125 Bayesian estimation theory. Kuai et al. (2010) analyzed both the  
126 Shannon information content and degrees of freedom in channel  
127 selection when retrieving CO<sub>2</sub> concentrations using thermal infrared  
128 remote sensing and indicated that 40 channels could contain 75% of  
129 the information from the total channels. Cyril et al. (2003) proposed  
130 the optimal sensitivity profile method based on the sensitivity of  
131 different atmospheric components. Lupu et al. (2012) used degrees  
132 of freedom for signals (DFS) to estimate the amount of information

133 contained in observations in the context of observing system  
134 experiments. In addition, the singular value decomposition method  
135 has also been widely used for channel selection (Prunet et al., 2010;  
136 Zhang et al., 2011; Wang et al., 2014). In 2017, Chang et al. (2017)  
137 selected a new set of Infrared Atmospheric Sounding Interferometer  
138 (IASI) channels using the channel score index (CSI). Richardson et  
139 al. (2018) selected 75 from 853 channels based on the high  
140 spectral-resolution oxygen A-band instrument on NASA's Orbiting  
141 Carbon Observatory-2 (OCO-2), using information content analysis  
142 to retrieve the cloud optical depth, cloud properties, and position.

143 Today's main methods for channel selection use only the  
144 weighting function to study appropriate numerical methods, such as  
145 the data precision matrix method (Menke, 1984), singular value  
146 decomposition method (Prunet et al., 2010; Zhang et al., 2011; Wang  
147 et al., 2014), and the Jacobi method (Aires et al., 1999; Rabier et al.,  
148 2010). The use of the methods allows sensitive channels to be  
149 selected. The above-mentioned studies also take into account the  
150 sensitivity of each channel to atmospheric parameters during channel  
151 selection, while ignoring some factors that impact retrieval results.  
152 The accuracy of retrieval results depends not only on the channel  
153 weighting function but also on the channel noise, background field,  
154 and the retrieval algorithm.

155 Currently, information content is often employed in channel  
156 selection. During retrieval, this method delivers the largest amount  
157 of information for the selected channel combination (Rodgers, 1996;  
158 Du et al., 2008; He et al., 2012; Richardson et al., 2018). This  
159 method has made great breakthroughs in both theory and practice,  
160 and the concept of information content itself does consider all the  
161 height dependencies of the kernel matrix  $K$  (Rodgers, 2000).  
162 However, earlier works have neglected the height dependencies of  $K$   
163 for simplicity. This paper uses the atmospheric retrievable index  
164 (ARI) as the index, which is based on information content (Du et al.,  
165 2008; Richardson et al. 2018). Channel selection is made at different  
166 heights, and an effective channel selection scheme is proposed  
167 which fully considers various factors, including the influence of  
168 different channels on the retrieval results at different heights. This  
169 ensures the best accuracy of the retrieval product when using the  
170 selected channel. In addition, statistical inversion comparison  
171 experiments are used to verify the effectiveness of the method.

172

## 173 **2 Channel selection indicator, scheme and method**

### 174 **2.1 Channel selection indicator**

175 According to the concept of information content, the information  
176 content contained in a selected channel of a hyperspectral instrument



177 can be described as H (Rodgers, 1996; Rabier et al., 2010). The final  
 178 expression of H is:

179

$$H = -\frac{1}{2} \ln |\hat{S} S_a^{-1}|$$

180

$$181 \quad = -\frac{1}{2} \ln |(S_a - S_a K^T (K S_a K^T + S_\varepsilon)^{-1} K S_a) S_a^{-1}|, \quad (1)$$

182

183 where  $S_a$  is the error covariance matrix of the background or the  
 184 estimated value of atmospheric profile,  $S_\varepsilon$  represents the  
 185 observation error covariance matrix of each hyperspectral detector  
 186 channel,  $\hat{S} = (S_a - S_a K^T (K S_a K^T + S_\varepsilon)^{-1} K S_a)$  denotes the  
 187 covariance matrix after retrieval, K is the weighting function matrix.

188 In order to describe the accuracy of the retrieval results visually  
 189 and quantitatively, the atmospheric retrievable index (ARI), p, (Du et  
 190 al., 2008) is defined as follows:

191

$$192 \quad p = 1 - \exp\left(\frac{1}{2n} \ln |\hat{S} S_a^{-1}|\right), \quad (2)$$

193

194 Assuming that before and after retrieval, the ratio of the root mean  
 195 square error of each element in the atmospheric state vector is 1-p,  
 196 then  $|\hat{S} S_a^{-1}| = (1 - p)^{2n}$  is derived. By inverting the equation, the  
 197 ARI that is p can be obtained in Eq. (2), which indicates the relative

198 portion of the error that is eliminated by retrieval. In fact, before and  
199 after retrieval, the ratio of the root mean square error of each element  
200 cannot be  $1-p$ . Therefore,  $p$  defined by Eq. (1) is actually an overall  
201 evaluation of the retrieval result.

202

## 203 **2.2 Channel selection scheme**

204 The principle of channel selection is to find the optimum channel  
205 combination after numbering the channels. This combination makes  
206 the information content,  $H$ , or the ARI defined in this paper as large  
207 as possible, in order to maintain the highest possible accuracy in the  
208 retrieval results.

209 Let there be  $M$  layers in the vertical direction of the atmosphere  
210 and  $N$  satellite channels. Selecting  $n$  from  $N$  channels, there will be  
211  $C_N^n$  combinations in each layer, leading  $C_N^n$  calculations to get  $C_N^n$   
212 kinds of  $p$  results. Furthermore, there are  $M$  layers in the vertical  
213 direction of the atmosphere. Therefore, the entire atmosphere must  
214 be calculated  $M \cdot C_N^n$  times. However, the calculation  $M \cdot C_N^n$  times  
215 will be particularly large, which makes this approach impractical in  
216 calculating  $p$  for all possible combinations. Therefore, it is necessary  
217 to design an effective calculation scheme, and such a scheme, i.e., a  
218 channel selection method, using iteration is proposed, called the  
219 “sequential absorption method” (Dudhia et al., 2002; Du et al., 2008).

220 The method's main function is to select ("absorb") channels one by  
 221 one, taking the channel with the maximum value of p. Through n  
 222 iterations, n channels can be selected as the final channel  
 223 combination. The steps are as follows:

224 (1) The expression of information content in a single channel:

225 First, we use only one channel for retrieval. A row vector, k, in the  
 226 weighting function matrix, K, is a weighting function corresponding  
 227 to the channel. After observation in this channel, the error covariance  
 228 matrix is:

$$229 \hat{S} = S_a - S_a k^T (s_\varepsilon + k S_a k^T)^{-1} k S_a. \quad (3)$$

230 It should be noted that  $(s_\varepsilon + k S_a k^T)$  is a scalar value in Eq. (3),  
 231 so Eq. (3) can be converted to:

$$232 \hat{S} = \left( I - \frac{S_a k^T k}{(s_\varepsilon + k S_a k^T)} \right) S_a = \left( I - \frac{(k S_a)^T k}{(s_\varepsilon + k (k S_a)^T)} \right) S_a. \quad (4)$$

233 Substituting Eq. (4) into Eq. (2) gives:

$$234 p = 1 - \exp\left(\frac{1}{2n} \ln\left(\left| I - \frac{(k S_a)^T k}{(s_\varepsilon + k (k S_a)^T)} \right|\right)\right). \quad (5)$$

235

236 (2) Simplification of Eq. (5) p matrix:

237 Since  $S_a$  and  $S_\varepsilon$  are positive definite symmetric matrixes, it can  
 238 be decomposed into  $S_a = (S_a^{1/2})^T (S_a^{1/2})$  and  $S_\varepsilon = (S_\varepsilon^{1/2})^T (S_\varepsilon^{1/2})$ .

239

$$240 \text{ Define } R = S_\varepsilon^{1/2} K S_a^{1/2}. \quad (6)$$

241

242 The matrix  $R$  can then be regarded as a weighting function matrix,  
243 normalized by the observed error and a priori uncertainty. A row  
244 vector of  $R$ ,  $r = s_\varepsilon^{-1/2} k S_a^{1/2}$ , represents the normalized weighting  
245 function matrix of a single channel. Substituting  $r$  into Eq. (5) gives:

246

$$247 \quad p = 1 - \exp\left(\frac{1}{2n} \ln \left( \left| I - \frac{rr^T}{1+rr^T} \right| \right)\right). \quad (7)$$

248

249 For arbitrary row vectors,  $a$  and  $b$ , using the matrix property  
250  $\det(I + a^T b) = 1 + ba^T$ , the new expression for  $p$  is:

251

$$\begin{aligned} p &= 1 - \exp\left(\frac{1}{2n} \ln \left( 1 - \frac{r^T r}{1 + r^T r} \right)\right) \\ 252 \quad &= 1 - \exp\left(\frac{1}{2n} \ln \left( \frac{1}{1+r^T r} \right)\right) \\ 253 \quad &= 1 - \exp\left(-\frac{1}{2n} \ln(1 + r^T r)\right). \end{aligned} \quad (8)$$

254

255 (3) Iteration in a single layer:

256 First, the iteration in a single layer requires the calculation of  $R$ .

257 According to  $S_a$ ,  $S_\varepsilon$ ,  $K$  and Eq. (6),  $R$  can be calculated. Second,  
258 using Eq. (8),  $p$  of each candidate channel can be calculated.

259 Moreover, the channel corresponding to maximum  $p$  is the selected  
260 channel for this iteration. After a channel has been selected,

261 according to Eq. (3) we can use  $\hat{S}$  to get  $S_a$  for the next iteration.  
262 Finally, channels which are not selected during this iteration are used  
263 as the candidate channels for the next iteration.

264 When selecting  $n$  from  $N$  channels, it is necessary to calculate  
265  $(N-n/2)n \approx Nn$   $p$  values, which is much smaller than  $C_N^n$ . In addition  
266 to high computational efficiency by using this method, another  
267 advantage is that all channels can be recorded in the order in which  
268 they are selected. In the actual application, if  $n'$  channels are  
269 needed, and  $n' < n$ , we will not need to select the channel again,  
270 but record the selected channel only.

271 (4) Iteration for different altitudes:

272 Because satellite channel sensitivity varies with height, repeating  
273 the iterative process of step (3), selects the optimum channels at  
274 different heights. Assuming there are  $M$  layers in the atmosphere and  
275 selecting  $n$  from  $N$  channels, it is necessary to calculate  $M \cdot (N -$   
276  $n/2)n \approx M \cdot Nn$   $p$  values, a much smaller number than  $M \cdot C_N^n$ . In  
277 this way, different channel sets can be used to evaluate  
278 corresponding height in the retrieved profiles.

279

## 280 **2.3 Statistical inversion method**

281 The inversion methods for the atmospheric temperature profiles can  
282 be summarized in two categories: statistical inversion and physical

283 inversion. Statistical inversion is essentially a linear regression  
284 model which uses a large number of satellite measurements and  
285 atmospheric parameters to match samples and calculate their  
286 correlation coefficient. Then, based on the correlation coefficient, the  
287 required parameters of the independent measurements obtained by  
288 the satellite are retrieved. Because the method does not directly solve  
289 the radiation transfer equation, it has the advantages of fast  
290 calculation speed. In addition, the solution is numerically stable,  
291 which makes it one of the highest precision methods (Chedin et al.,  
292 1985). Therefore, the statistical inversion method will be used for  
293 our channel selection experiment and a regression equation will be  
294 established.

295 According to an empirical orthogonal function, the atmospheric  
296 temperature (or humidity),  $T$ , and the brightness temperature,  $T_b$ , are  
297 expanded as:

298

$$299 \quad T = T^* \cdot A, \quad (9)$$

300

$$301 \quad T_b = T_b^* \cdot A, \quad (10)$$

302

303 where  $T^*$  and  $T_b^*$  are the eigenvectors of the covariance matrix of  
304 temperature (or humidity) and brightness temperature, respectively.

305 A and B stand for the corresponding expansion coefficient vectors of  
306 temperature (humidity) and brightness temperature.

307 Using the least squares method and the orthogonal property, the  
308 coefficient conversion matrix, V, is introduced:

309

$$310 \quad A = V \cdot B, \quad (11)$$

311

$$312 \quad \text{where } V = AB^T(BB^T)^{-1}. \quad (12)$$

313

314 Using the orthogonality, we get:

315

$$316 \quad B = (T_b^*)^T T_b, \quad (13)$$

317

$$318 \quad A = (T^*)^T T. \quad (14)$$

319

320 For convenience, the anomalies of the state vector (atmospheric  
321 temperature), T, and the observation vector (brightness temperature),  
322  $T_b$ , are taken:

323

$$324 \quad \hat{T} = \bar{T} + \hat{T}' = \bar{T} + GT_b' = \bar{T} + G(T_b - \bar{T}_b), \quad (15)$$

325

326 where  $\hat{T}$  stands for the retrieval atmospheric temperature.  $\bar{T}$  and

327  $\bar{T}_b$  are the corresponding average values of the elements,  
 328 respectively.  $\hat{T}'$  and  $T'_b$  represent the corresponding anomalies  
 329 of the elements, respectively.

330 Assuming there are k sets of observations, a sample anomaly  
 331 matrix with k vectors can be constructed:

332

$$333 \quad T' = (t'_1, t'_2, \dots, t'_k), \quad (16)$$

334

$$335 \quad T'_b = (t'_{b1}, t'_{b2}, \dots, t'_{bk}). \quad (17)$$

336

337 Define the inversion error matrix as:

338

$$339 \quad \delta = \bar{T} - \hat{T} = \hat{T}' - T'. \quad (18)$$

340

341 The retrieval error covariance matrix is:

342

$$\begin{aligned}
 343 \quad S_\delta &= \frac{1}{k-n-1} \delta \delta^T \\
 &= \frac{1}{k-n-1} (T' - GT'_b)(T' - GT'_b)^T \\
 344 \quad &= \frac{k-1}{k-n-1} (S_e - G^T S_{xy} - S_{xy} G^T + GS_y G^T), \quad (19)
 \end{aligned}$$

345

346 where

347



$$\begin{aligned}
348 \quad S_e &= \frac{1}{k-1} T' T' T, \\
349 \quad S_y &= \frac{1}{k-1} T_b' T_b' T, \\
350 \quad S_{xy} &= \frac{1}{k-1} T' T_b' T. \tag{20}
\end{aligned}$$

351

352  $S_e$  stands for the sample covariance matrix of  $T$ ,  $S_y$  denotes the  
353 sample covariance matrix of  $T_b$ , and  $S_{xy}$  represents the covariance  
354 matrix of  $T$  and  $T_b$ . The elements on the diagonal of the error  
355 covariance matrix,  $S_\delta$ , represent the retrieval error variance of  $T$ .  
356 The matrix  $G$  that minimizes the overall error variance is the least  
357 squares coefficient matrix of the regression equation (15), which  
358 meets the criteria:

359

$$360 \quad \delta^2 = \text{tr}(S_\delta) = \min. \tag{21}$$

361

362 Taking a derivative of Eq. (21) with respect to  $G$ ,  $\frac{\partial}{\partial G} \text{tr}(S_\delta) = 0 =$   
363  $(-2S_{xy} + 2GS_y)$ , which means that:

364

$$365 \quad G = S_{xy} S_y^{-1}. \tag{22}$$

366

367 Substituting Eq. (22) into Eq. (15) finally gives the least squares  
368 solution as:

369

$$370 \quad \hat{\mathbf{T}} = \bar{\mathbf{T}} + \mathbf{S}_{xy}\mathbf{S}_y^{-1}(\mathbf{T}_b - \bar{\mathbf{T}}_b). \quad (23)$$

371

372 It should be noted that the least squares solution obtained here  
373 aims to minimize the sum of the error variance for each element in  
374 the atmospheric state vector after retrieval for several times. At  
375 present, statistical multiple regression is widely used in the retrieval  
376 of atmospheric profiles based on atmospheric remote sensing data.  
377 As long as there are enough data,  $\mathbf{S}_{xy}$  and  $\mathbf{S}_y$  can be determined.

378

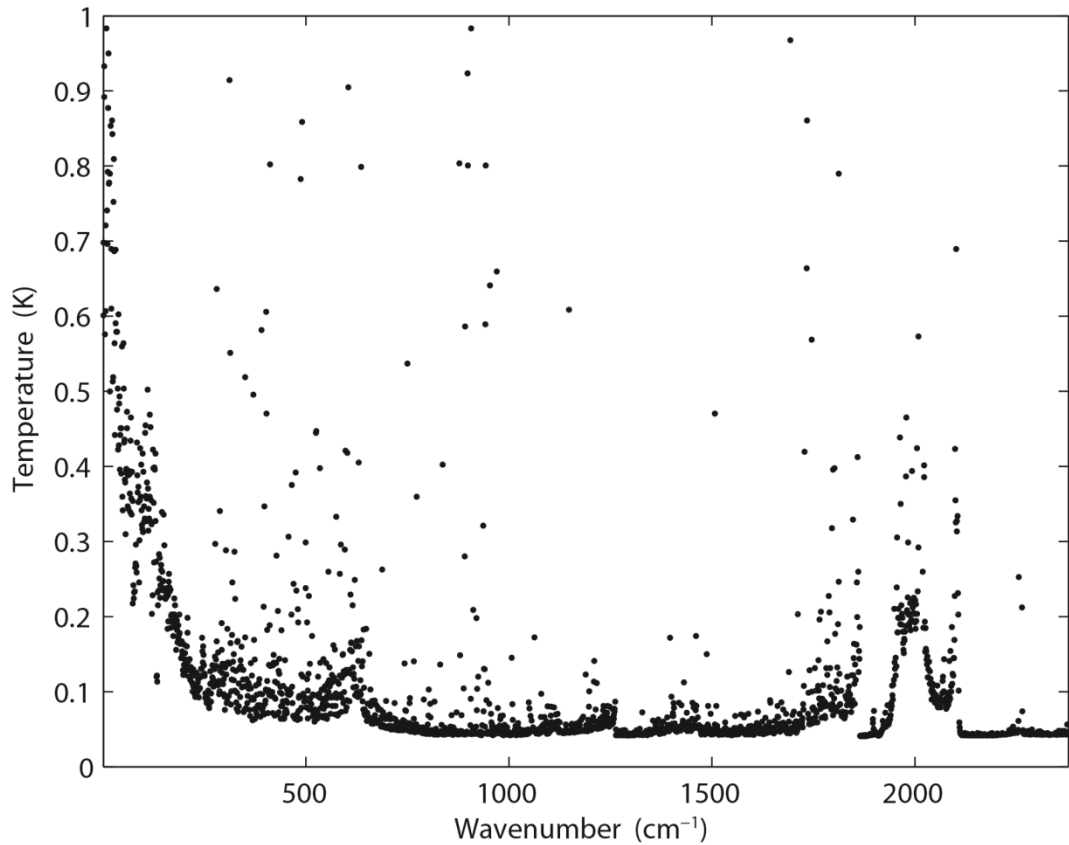
### 379 **3. Channel selection experiment**

#### 380 **3.1 Data and model**

381 The Atmospheric Infrared Sounder (AIRS) is primarily designed to  
382 measure the Earth's atmospheric water vapor and temperature  
383 profiles on a global scale (Aumann et al., 2003; Hoffmann and  
384 Alexander, 2009). AIRS is a continuously operating cross-track  
385 scanning sounder, consisting of a telescope that feeds an echelle  
386 spectrometer. The AIRS infrared spectrometer acquires 2378 spectral  
387 samples at a resolution  $\lambda/\Delta\lambda$ , ranging from 1086 to 1570, in three  
388 bands: 3.74  $\mu\text{m}$  to 4.61  $\mu\text{m}$ , 6.20  $\mu\text{m}$  to 8.22  $\mu\text{m}$ , and 8.8  $\mu\text{m}$  to 15.4  
389  $\mu\text{m}$ . The footprint size 13.5 km at nadir (Suskind et al., 2003). The  
390 spectral range includes 4.3  $\mu\text{m}$  and 15.5  $\mu\text{m}$  for important

391 temperature observation and CO<sub>2</sub>, 6.3 μm for water vapor, and 9.6  
392 μm for ozone absorption bands (Menzel et al., 2018). The root mean  
393 square error (RMSE) of the measured radiation is better than 0.2 K  
394 (Susskind et al., 2003). Moreover, global atmospheric profiles can be  
395 detected every day. Due to radiometer noise and faults, there are  
396 currently only 2047 effective channels. However, compared with  
397 previous infrared detectors, AIRS boasts a significant improvement  
398 in both the number of channels and spectral resolution (Aumann,  
399 1994; Huang et al., 2005; Li et al., 2005).

400 The root mean square error of an AIRS infrared channel is shown  
401 in Fig. 1, with black spots, indicating that not all the instrument  
402 channels possess a measurement error of less than 0.2 K. There are a  
403 few channels with extremely large measurement errors, which  
404 reduce the accuracy of prediction to some extent. Among them,  
405 some extremely large measurement errors reduce the accuracy of  
406 prediction to some extent (Susskind et al., 2003). At present, more  
407 than 300 channels have not been used because their errors exceed 1  
408 K. If data from these channels were to be used for retrieval, the  
409 accuracy of the retrieval could be reduced. Therefore, it is necessary  
410 to select a group of channels to improve the calculation efficiency  
411 and retrieval quality. In this paper we study channel selection for  
412 temperature profile retrieval by AIRS.



413

414 **Figure 1.** Root mean square error of AIRS infrared channel (black  
 415 spots).

416

417 For the calculation of radiative transfer and the weighting function  
 418 matrix,  $K$ , the RTTOV (Radiative Transfer for TOVS) v12 fast  
 419 radiative transfer model is used. Although initially developed for the  
 420 TOVS (TIROS Operational Vertical Sounder) radiometers, RTTOV  
 421 can now simulate around 90 different satellite sensors measuring in  
 422 the MW (microwave), IR (infrared) and VIS (visible) regions of the  
 423 spectrum (Saunders et al., 2018). The model allows rapid  
 424 simulations (1 ms for 40 channel ATOVS (Advanced TOVS) on a  
 425 desktop PC) of radiances for satellite visible, infrared, or microwave

426 nadir scanning radiometers given atmospheric profiles of  
427 temperature and trace gas concentrations, and cloud and surface  
428 properties. The only mandatory gas included as a variable for  
429 RTTOV v12 is water vapor. Optionally, ozone, carbon dioxide,  
430 nitrous oxide, methane, carbon monoxide, and sulfur dioxide can be  
431 included, with all other constituents assumed to be constant. RTTOV  
432 can accept input profiles on any defined set of pressure levels. The  
433 majority of RTTOV coefficient files are based on the 54 levels (see  
434 Table A1 in Appendix A), ranking from 1050 hPa to 0.01 hPa,  
435 though coefficients for some hyperspectral sounders are also  
436 available on 101 levels.

437 In order to correspond to the selected profiles, the atmosphere is  
438 divided into 137 layers, each of which contains corresponding  
439 atmospheric characteristics, such as temperature, pressure, and the  
440 humidity distribution. Each element in the weighting function matrix  
441 can be written as  $\partial y_i / \partial x_j$ . The subscript  $i$  is used to identify the  
442 satellite channel, and the subscript  $j$  is used to identify the  
443 atmospheric variable. Therefore,  $\partial y_i / \partial x_j$  indicates the variation in  
444 brightness temperature in a given satellite channel, when a given  
445 atmospheric variable in a given layer changes. We are thus able to  
446 establish which layer of the satellite channel is particularly sensitive  
447 to which atmospheric characteristic (temperature, various gas

448 contents) in the vertical atmosphere. The RTTOV\_K (the K mode),  
449 is used to calculate the matrix  $H(X_0)$  (Eq. (1)) for a given  
450 atmospheric profile characteristic.

451

### 452 **3.2 Channel selection comparison experiment and results**

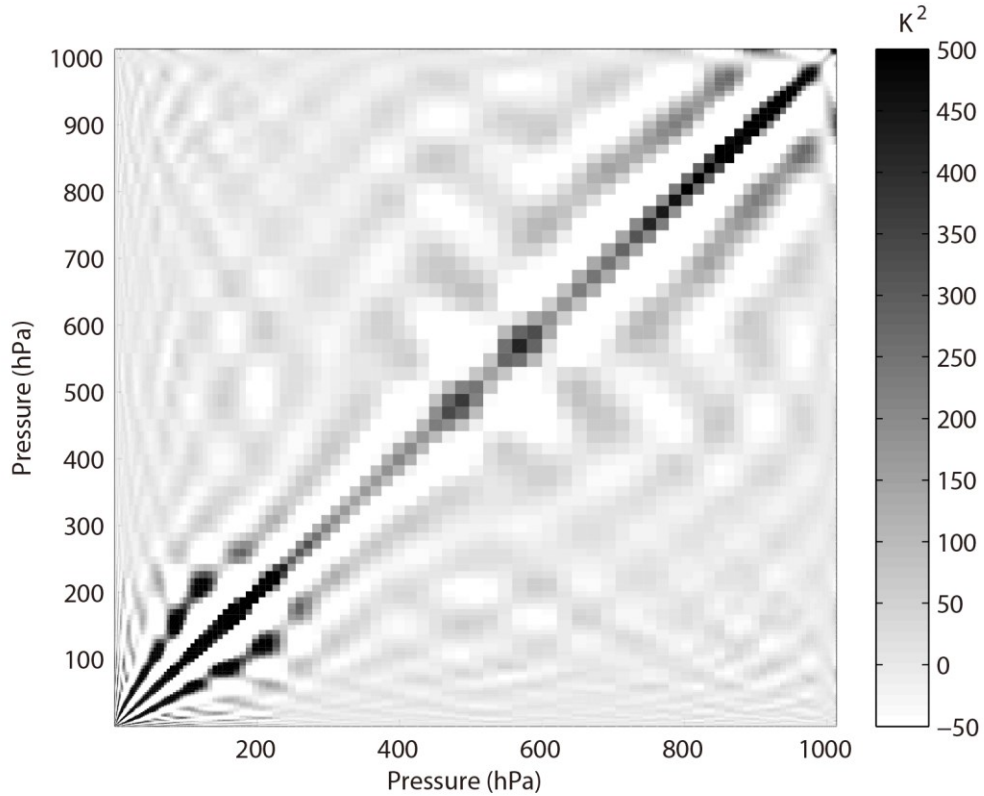
453 In order to verify the effectiveness of the method, three sets of  
454 comparison experiments were conducted. First, 324 channels used  
455 by the EUMETSAT Satellite Application Facility on Numerical  
456 Weather Prediction (NWP SAF) were selected. NCS is short for  
457 NWP channel selection in this paper. NCS were released by the  
458 NWPSAF 1DVar (one-dimensional variational analysis) scheme, in  
459 accordance with the requirements of the NWPSAF (Saunders et al.,  
460 2018). Second, 324 channels were selected using the information  
461 capacity method. This method was adopted by Du et al. (2008)  
462 without the consideration of layering. PCS is short for primary  
463 channel selection in this paper.

464 Third,  $324 \times M$  channels were selected using the information  
465 capacity method for the M layer atmosphere. ICS is short for  
466 improved channel selection in this paper. In order to verify the  
467 retrieval effectiveness after channel selection, statistical inversion  
468 comparison experiments were performed using 5000 temperature  
469 profiles provided by the ECMWF dataset, which will be introduced

470 in Sect. 4.

471 The observation error covariance matrix,  $S_{\varepsilon}$ , in the experiment is  
472 provided by NWP SAF 1Dvar. In general, it can be converted to a  
473 diagonal matrix, the elements of which are the observation error  
474 standard deviation of each hyperspectral detector channel, which is  
475 the square of the root mean square error for each channel. The root  
476 mean square error of the AIRS channels is shown in Fig. 1. The error  
477 covariance matrix of the background,  $S_a$ , is calculated using 5000  
478 samples of the IFS-137 data provided by the ECMWF dataset (The  
479 detailed information will be introduced in Sect. 4). The last access  
480 date is April 26th, 2019 (download address:  
481 <https://www.nwpsaf.eu/site/update-137-level-nwp-profile-dataset/>,  
482 2019). The covariance matrix of temperature is shown in Fig. 2. The  
483 results are consistent with the previous study by Du et al. (2008).

484



485

486 **Figure 2.** Error covariance matrix of temperature (shaded).

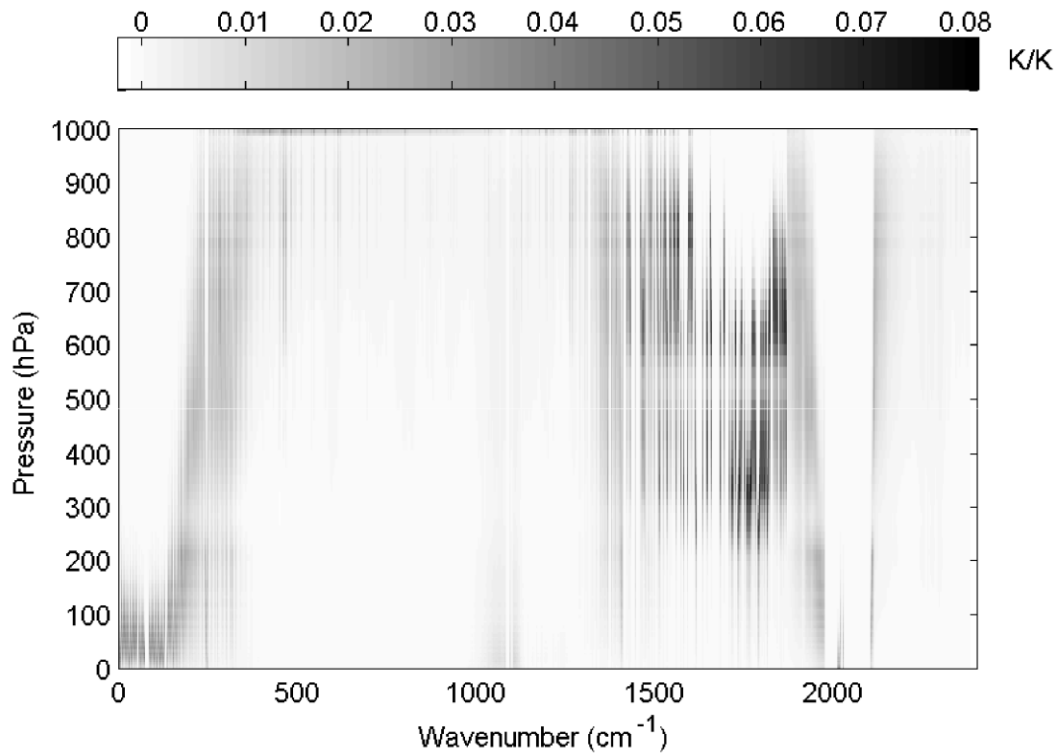
487

488 The reference atmospheric profiles are from the IFS-137 database,  
 489 and the temperature weighting function matrix is calculated using  
 490 the RTTOV\_K mode, as shown in Fig. 3; the results are consistent  
 491 with those of the previous study by Du et al. (2008). For the  
 492 air-based passive atmospheric remote sensing studied in this paper,  
 493 when the same channel detects the atmosphere from different  
 494 observation angles, the value of the weighting function matrix  $K$   
 495 changes due to the limb effect. The goal of this section is focusing  
 496 on the selection methods of selecting channels; therefore the biases  
 497 produced from different observation angles can be ignored.



498

499

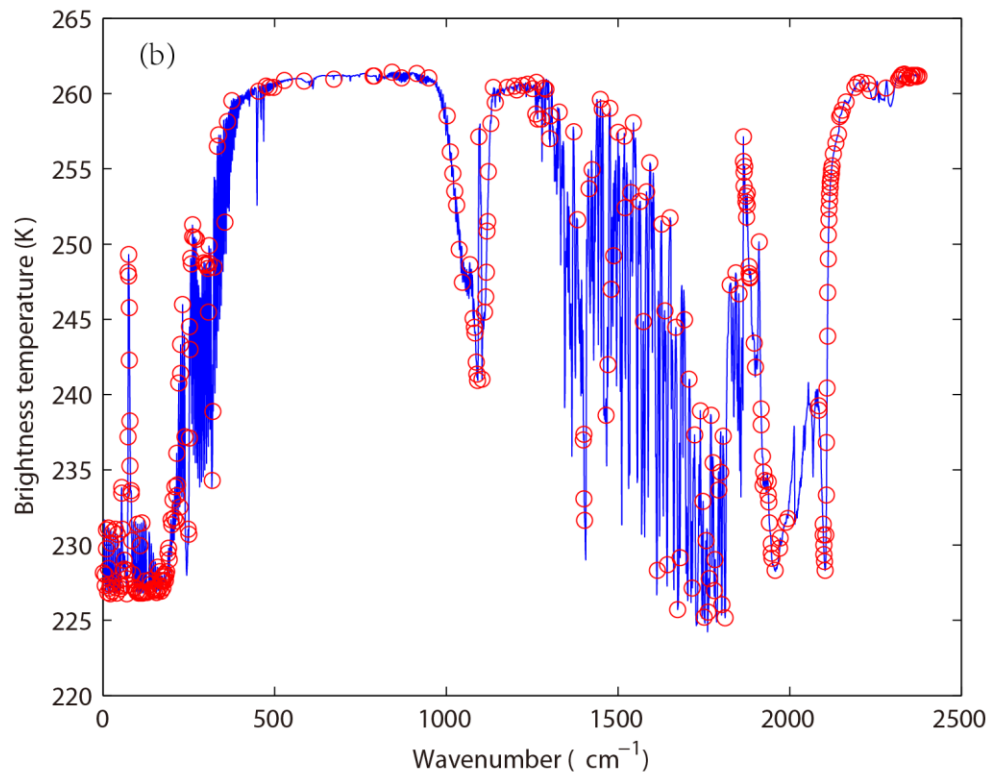
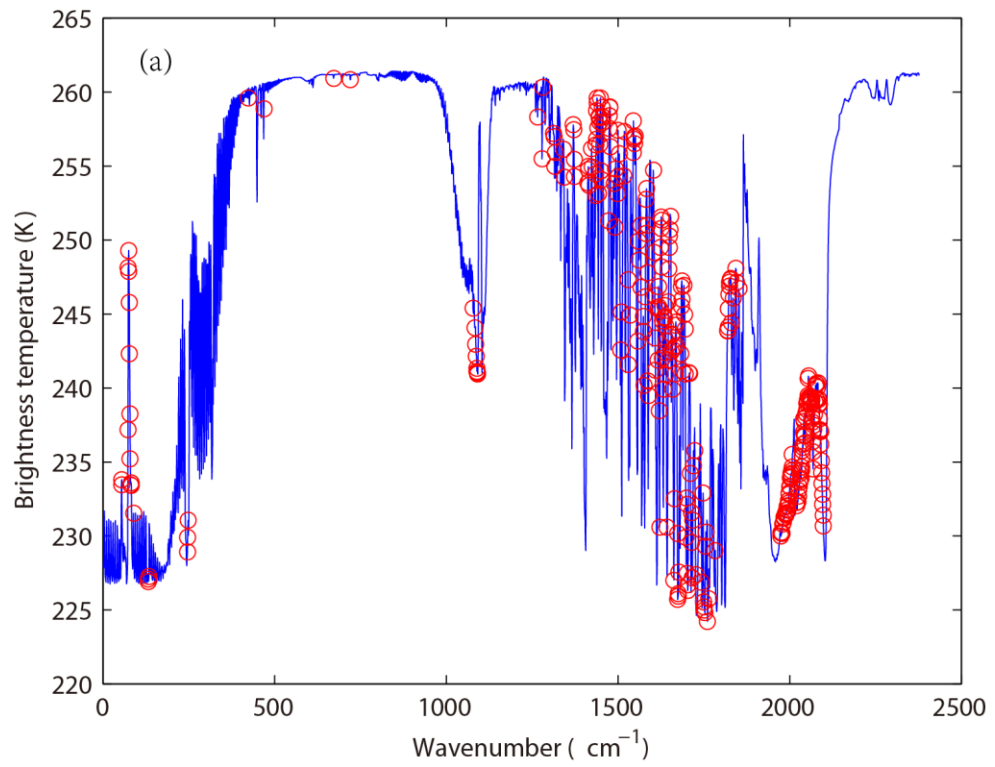


500 **Figure 3.** Temperature weighting function matrix (shaded).

501

502 In order to verify the effectiveness, the distribution of 324  
503 channels, without considering layering, in the AIRS brightness  
504 temperature spectrum is indicated in Fig. 4. The background  
505 brightness temperature is the simulated AIRS observation brightness  
506 temperature, which is from the atmospheric profile in RTTOV put  
507 into the model. Figure 4(a) shows the 324 channels selected by PCS,  
508 while Fig. 4(b) shows the 324 channels selected by NCS.

509



510

511 **Figure 4.** The distribution of different channel selection methods

512 without considering layering in the AIRS brightness temperature

513 spectrum (blue line). (a) 324 channels selected by PCS (red circles).  
514 (b) 324 channels selected by NCS (red circles).

515 Without considering layering, the main differences between the  
516 324 channels selected by PCS and NCS are as follows: (1) When the  
517 wavenumber approaches 1000, the wavelength is 10  $\mu\text{m}$  ( $1/1000$   
518  $\text{cm}^{-1}$ ). Near this band, fewer channels are selected by PCS because  
519 the retrieval of ground temperature is considered by NCS; (2) When  
520 the wavenumber is near 1200, the wavelength is 9  $\mu\text{m}$  ( $1/1200 \text{ cm}^{-1}$ ).  
521 Near this band, no channels are selected by PCS because the  
522 retrieval of  $\text{O}_3$  is not considered in this paper; (3) When the  
523 wavenumber approaches 1500, the wavelength is 6.7  $\mu\text{m}$  ( $1/1500$   
524  $\text{cm}^{-1}$ ). As is known, the spectral range from 6  $\mu\text{m}$  to 7  $\mu\text{m}$   
525 corresponds to water vapor absorption bands, but fewer channels are  
526 selected by NCS; (4) When the wavenumber is close to 2000, it  
527 derives a wavelength of 5  $\mu\text{m}$  ( $1/2000 \text{ cm}^{-1}$ ), which includes 4.2  $\mu\text{m}$   
528 for  $\text{N}_2\text{O}$  and 4.3  $\mu\text{m}$  for  $\text{CO}_2$  absorption bands. As is shown in Fig. 4,  
529 fewer channels are selected by PCS in those bands. PCS is favorable  
530 for atmospheric temperature observation in the high temperature  
531 zone. Because 4.2  $\mu\text{m}$  and 4.3  $\mu\text{m}$  bands are sensitive to high  
532 temperature, the higher temperature is, the better observation can be  
533 obtained; (5) In the near infrared area, the wavenumber exceeds  
534 2200, deriving a wavelength of less than 4  $\mu\text{m}$  ( $1/2000 \text{ cm}^{-1}$ ). A

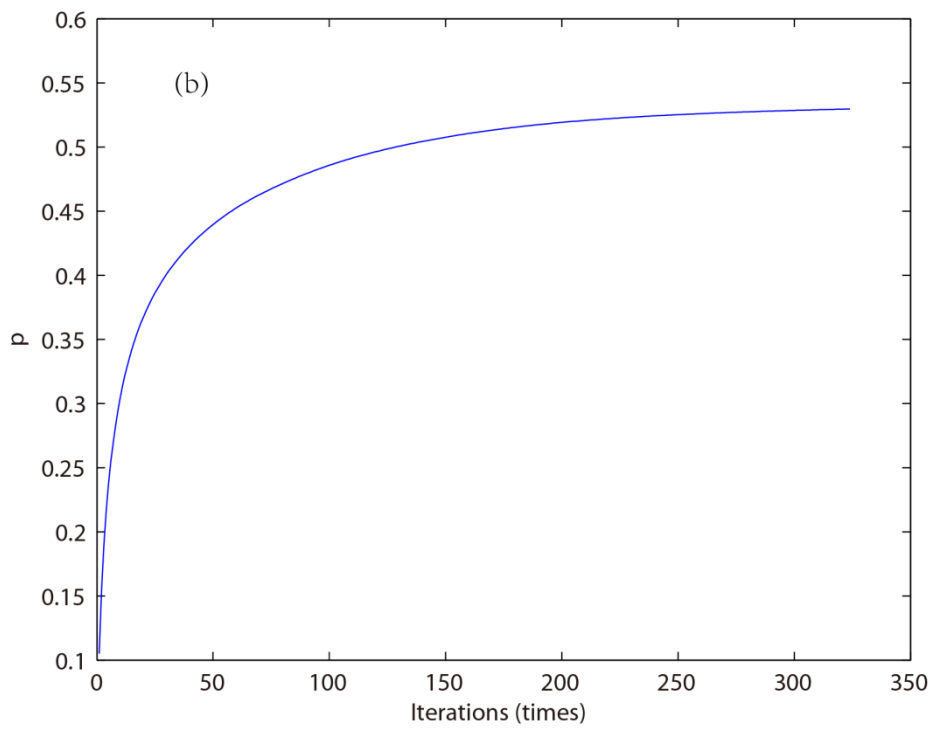
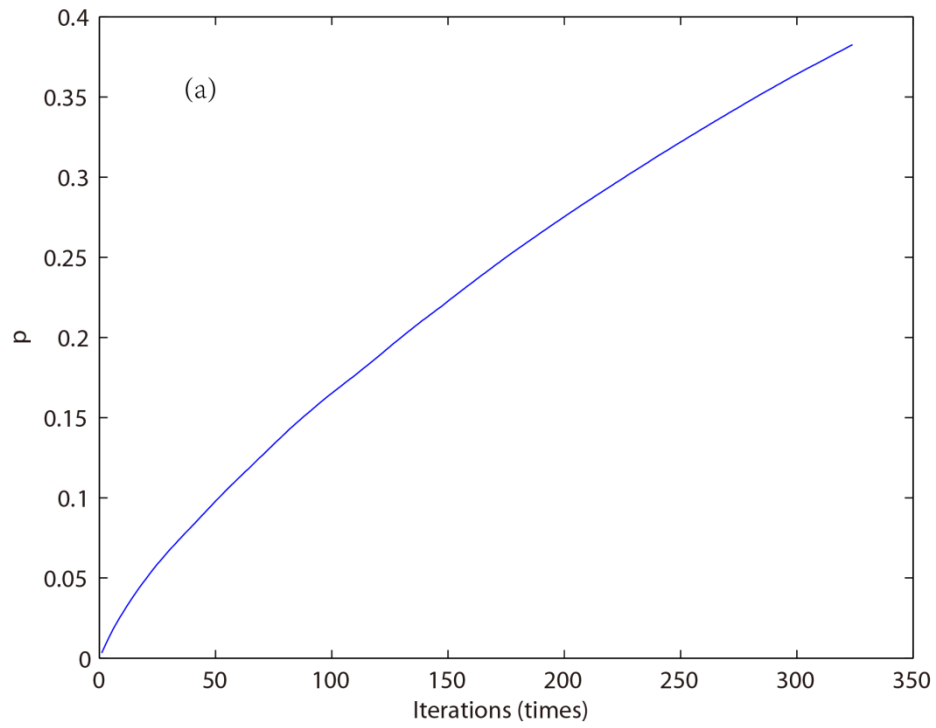
535 small number of channels is selected by NCS, but no channels are  
536 selected by PCS.

537 Above all, the information content used in this paper only takes  
538 the temperature profile retrieval into consideration, so the channel  
539 combination of PCS is inferior to that of NCS for the retrieval of  
540 surface temperature and the O<sub>3</sub> profile. The advantages of the  
541 channel selection method based on information content in this paper  
542 are mainly reflected in: (1) Stratosphere and mesosphere is less  
543 affected by the ground surface, so the retrieval result of PCS is better  
544 than that of NCS. (2) Due to the method selected in this paper there  
545 are more channels at 4.2 μm for N<sub>2</sub>O and 4.3 μm for CO<sub>2</sub> absorption  
546 bands; the channel combination of PCS is better than that of NCS for  
547 atmospheric temperature observation to the higher temperature.

548 By comparing channel selection without considering layering,  
549 we note the general advantages and disadvantages of PCS and NCS  
550 for the retrieval of temperature and can improve the channel  
551 selection scheme. First, the retrieval of the temperature profile for  
552 324 channels selected by PCS is obtained. The relationship between  
553 the number of iterations and the ARI is shown in Fig. 5.

554

555



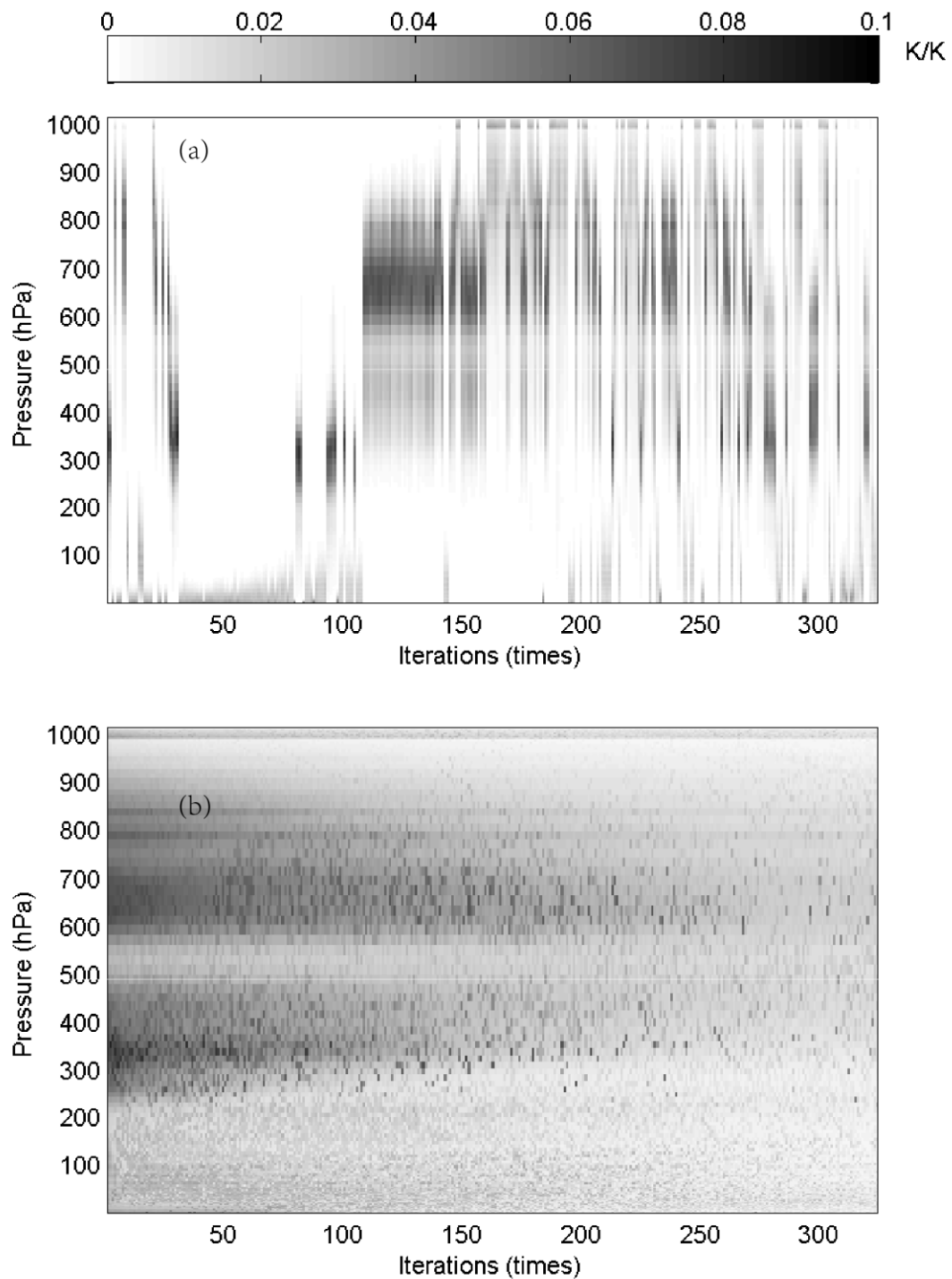
556 **Figure 5.** The relationship between the number of iterations and ARI.

557 (a) PCS. (b) ICS.

558

559 The ARI for PCS tends to be 0.38 and is not convergent, so the  
560 PCS method needs to be improved. In this paper, the atmosphere is  
561 divided into 137 layers, and based on the information content and  
562 iteration, 324 channels are selected for each layer. Then, the  
563 temperature profile of each layer can be retrieved based on statistical  
564 inversion (see at Sect. 4). The relationship between the number of  
565 iterations and the ARI for ICS is shown in Fig. 5b. When the number  
566 of iterations approaches 100, the ARI of ICS tends to be stable, and  
567 reach to 0.54. Thus, in terms of the ARI and convergence, the ICS  
568 method is better than that of PCS.

569 Furthermore, because an iterative method is used to select  
570 channels, the order of each selected channel is determined by the  
571 contribution from the ARI. The weighting function matrix of the top  
572 324 selected channels, according to channel order, is shown in Fig.  
573 6.



575 **Figure 6.** The relationship between the number of iterations and the  
 576 weighting function of the top 324 selected channels (shaded). (a)  
 577 ICS. (b) PCS.

578

579 As illustrated in Fig. 6, in the first 100 iterations, the distribution  
580 of the temperature weighting function for PCS is relatively scattered;  
581 it does not reflect continuity between the adjacent layers of the  
582 atmosphere. Besides, the ICS result is better than that of PCS,  
583 showing that: (1) the distribution of the temperature weighting  
584 function is more continuous and reflects the continuity between  
585 adjacent layers of the atmosphere; (2) regardless of the number of  
586 iterations, the maximum value of the weighting function is stable  
587 near 300–400 hPa and 600–700 hPa, without scattering, which is  
588 closer to the situation in real atmosphere.

589

#### 590 **4. Statistical multiple regression experiment**

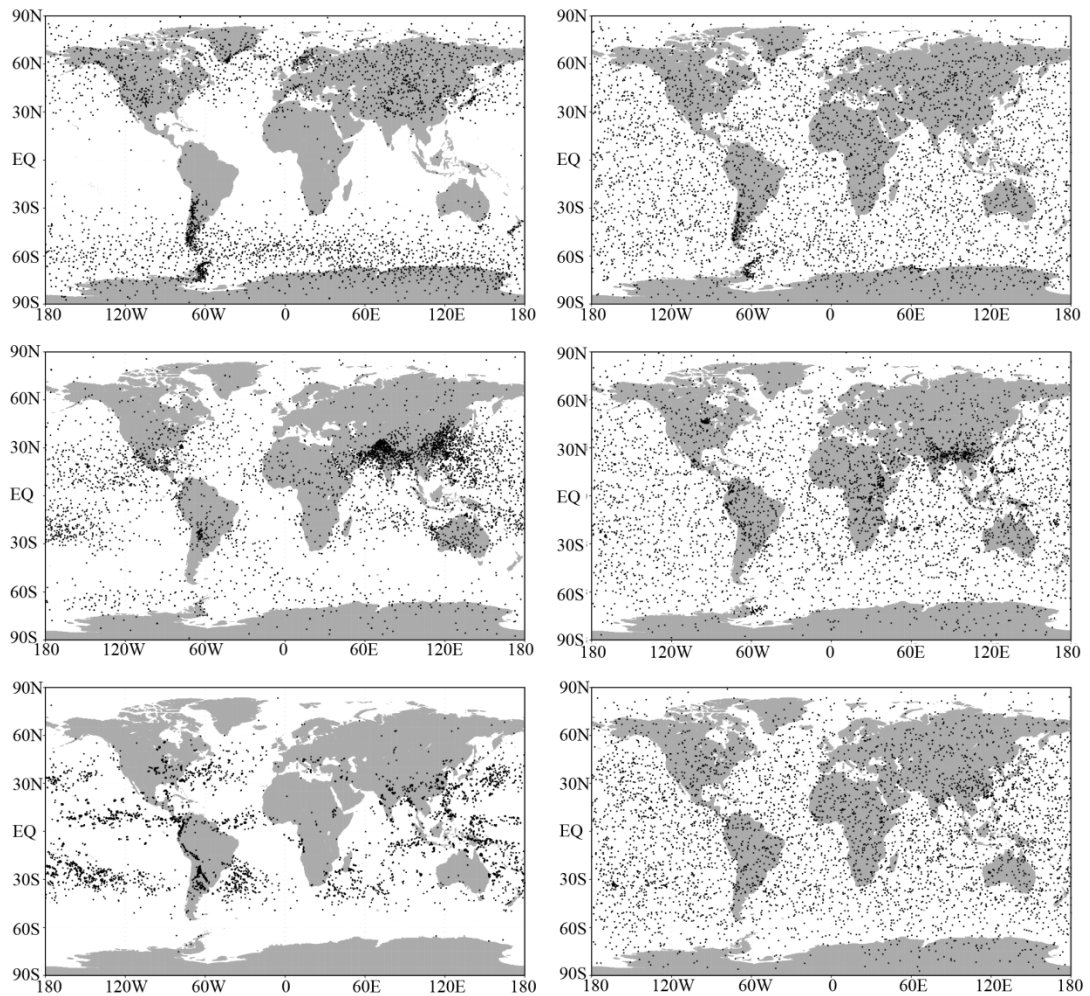
##### 591 **4.1 Temperature profile database**

592 A new database including a representative collection of 25,000  
593 atmospheric profiles from the European Centre for Medium-range  
594 Weather Forecasts (ECMWF) was used for the statistical inversion  
595 experiments. The profiles were given in a 137-level vertical grid  
596 extending from the surface up to 0.01 hPa. The database was divided  
597 into five subsets focusing on diverse sampling characteristics such as  
598 temperature, specific humidity, ozone mixing ratio, cloud  
599 condensates, and precipitation. In contrast with earlier releases of the



600 ECMWF diverse profile database, the 137-level database places  
601 greater emphasis on preserving the statistical properties of sampled  
602 distributions produced by the Integrated Forecasting System (IFS)  
603 (Eresmaa and McNally, 2014; Brath et al., 2018). IFS-137 spans the  
604 period from September 1, 2013 to August 31, 2014. There are two  
605 operational analyses each day (at 00z and 12z), and approximately  
606 13 000 atmospheric profiles over the ocean. The pressure levels  
607 adopted for IFS-137 are shown in Table A2 (see Table A2 in  
608 Appendix A).

609 The locations of selected profiles of temperature, specific  
610 humidity, and cloud condensate subsets of the IFS-91 and IFS-137  
611 databases are plotted on the map in Fig. 7. In the IFS-91 database,  
612 the sampling is fully determined by the selection algorithm, which  
613 makes the geographical distributions very inhomogeneous. Selected  
614 profiles represent those regions where gradients of the sampled  
615 variable are the strongest: in the case of temperature, mid- and  
616 high-latitudes dominate, while humidity and cloud condensate  
617 subsets concentrate at low latitudes. However, the IFS-137 database  
618 shows a much more homogeneous spatial distribution in all the  
619 sampling subsets, which is a consequence of the randomized  
620 selection.

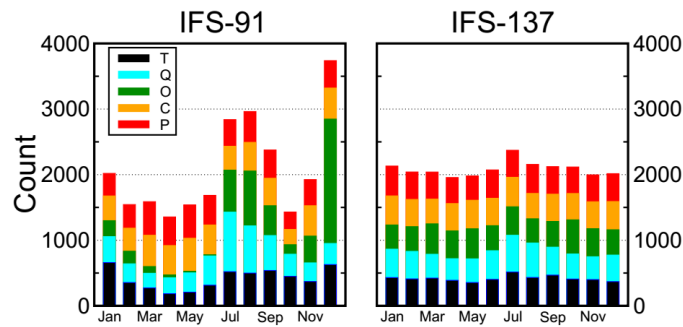


622 **Figure 7.** Locations of selected profiles in the temperature (top),  
 623 specific humidity (middle), and cloud condensate (bottom), sampled  
 624 subsets of the IFS-91 (left) and IFS-137 (right) databases (from  
 625 <https://www.nwpsaf.eu/site/update-137-level-nwp-profile-dataset/> ,  
 626 2019).

627

628 The temporal distribution of the selected profiles is illustrated in Fig.  
 629 8. The coverage of the IFS-137 data set is more homogeneous than

630 the IFS-91 data set. Moreover, the IFS-137 database supports the  
 631 mode with input parameters, such as detection angle, 2 m  
 632 temperature, and cloud information. Therefore, it is feasible to use  
 633 the selected samples in a statistical multiple regression experiment.



634 **Figure 8.** Distribution of profiles within the calendar months in  
 635 IFS-91 (left) and IFS-137 (right) databases. Different subsets are  
 636 shown in different colors. Black parts stand for temperature. Blue  
 637 parts represent specific humidity. Green parts indicate ozone subset.  
 638 Orange parts stand for cloud condensate. Red parts represent  
 639 precipitation. The last access date is April 26th, 2019. (from  
 640 <https://www.nwpsaf.eu/site/update-137-level-nwp-profile-dataset/> ,  
 641 2019).

642

#### 643 **4.2 Experimental scheme**

644 In order to verify the retrieval effectiveness of ICS, 5000  
 645 temperature profiles provided by the IFS-137 were used for  
 646 statistical inversion comparison experiments. The steps are as  
 647 follows:

648 (1) 5000 profiles and their corresponding surface factors,  
649 including surface air pressure, surface temperature, 2 m temperature,  
650 2 m specific humidity, 10 m wind speed. are put into the RTTOV  
651 mode. Then, the simulated AIRS spectra are obtained.

652 (2) The retrieval of temperature is carried out in accordance with  
653 Eq. (23). The 5000 profiles are divided into two groups. The first  
654 group of 2500 profiles is used to obtain the regression coefficient,  
655 and the second group of 2500 is used to test the result.

656 (3) Verification of the results. The test is carried out based on the  
657 standard deviation between the retrieval value and the true value.

658

### 659 **4.3 Results and Discussion**

660 For the statistical inversion comparison experiments, the standard  
661 deviation of temperature retrieval is shown in Fig. 9. First, because  
662 PCS does not take channel sensitivity as a function of height into  
663 consideration, the retrieval result of PCS is inferior to that of ICS.  
664 Second, by comparing the results of ICS and NCS we found that  
665 below 100 hPa, since the method used in this paper considers near  
666 ground to be less of an influencing factor, the channel combination  
667 of ICS is slightly inferior to that of NCS, but the difference is small.

668 From 100 hPa to 10 hPa, the retrieval temperature of ICS in this  
669 paper is consistent with that of NCS, slightly better than the channel

670 selected for NCS. From 10 hPa to 0.02 hPa, near the space layer, the  
671 retrieval temperature of ICS is better than that of NCS. In terms of  
672 the standard deviation, the channel combination of ICS is slightly  
673 better than that of PCS from 100 hPa to 10 hPa. From 10 hPa to 0.02  
674 hPa, the standard deviation of ICS is lower than that of NCS at about  
675 1 K, meaning that the retrieval result of ICS is better than that of  
676 NCS.

677 In order to further illustrate the effectiveness of ICS, the mean  
678 improvement value of the ICS and its percentages compared with the  
679 PCS and NCS at different heights are shown in Table 1. Because  
680 PCS does not take channel sensitivity as a function of height into  
681 consideration, the retrieval result of PCS is inferior to that of ICS. In  
682 general, the accuracy of the retrieval temperature of ICS is improved.  
683 Especially, from 100 hPa to 0.01 hPa, the mean value of ICS is  
684 evidently improved by more than 0.5 K which means the accuracy  
685 can be improved by more than 11%. By comparing the results of ICS  
686 and NCS we found that below 100 hPa, since the method used in this  
687 paper considers near ground to be less of an influencing factor, the  
688 channel combination of ICS is slightly inferior to that of NCS, but  
689 the difference is small. From 100 hPa to 0.01 hPa, the mean value of  
690 ICS is improved by more than 0.36 K which means the accuracy can  
691 be improved by more than 9.6%.

692

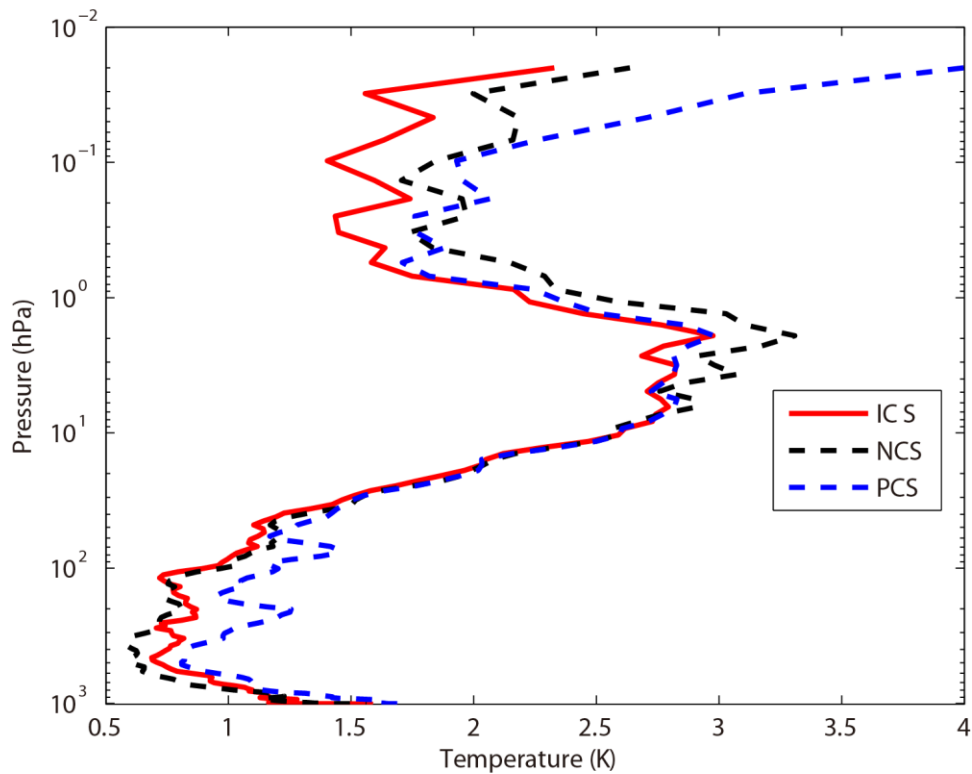
693 **Table 1.** The mean improvement value of the ICS and its  
694 percentages compared with the PCS and NCS at different heights.

Pressure	Improved mean value /Percentage compared with PCS	Improved value /Percentage compared with NCS
hPa	K/%	K/%
surface-100hPa	0.24/10.77%	-0.04/-3.27%
100hPa-10hPa	0.15/5.08%	0.06/2.4%
10hPa-1hPa	0.04/0.64%	0.17/2.99%
1hPa-0.01hPa	0.52/11.92%	0.36/9.57%

695

696 This is because, as shown in Fig. 4: (1) Stratosphere and  
697 mesosphere is less affected by the ground surface, so the retrieval  
698 result of PCS is better than that of NCS. (2) Due to the method  
699 selected in this paper, there are more channels at 4.2  $\mu\text{m}$  for  $\text{N}_2\text{O}$  and  
700 4.3  $\mu\text{m}$  for  $\text{CO}_2$  absorption bands, and the channel combination of  
701 PCS is superior to that of NCS for atmospheric temperature  
702 observation in the high temperature zone. Moreover, ICS takes  
703 channel sensitivity as a function of height into consideration, so its  
704 retrieval result is improved.

705



706

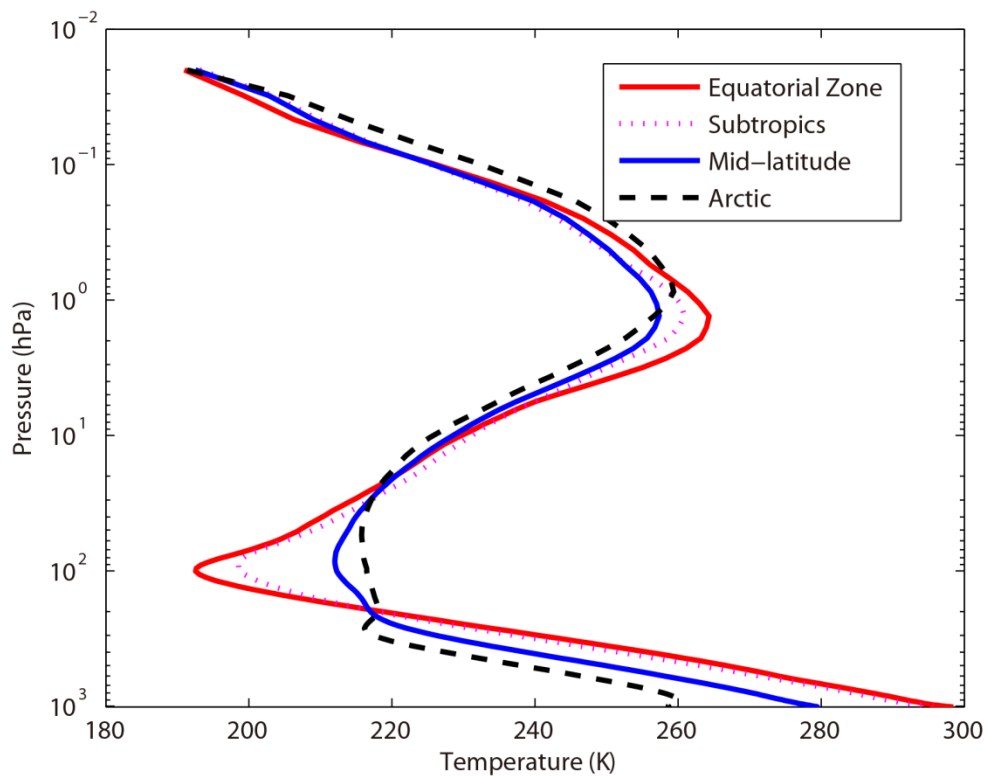
707 **Figure 9.** The temperature profile standard deviation of statistical  
 708 inversion comparison experiments. Red line indicates the result of  
 709 ICS. Black dotted line stands for the result of NCS. Blue dotted line  
 710 represents the result of PCS.

711

712 **5 Statistical inversion comparison experiments in four typical**  
 713 **regions**

714 The accuracy of the retrieval temperature varies from place to place  
 715 and changes with atmospheric conditions. Therefore, in order to  
 716 further compare the inversion accuracy under different atmospheric  
 717 conditions, this paper has divided the atmospheric profile from the  
 718 IFS-137 database introduced in Sect. 4 into four regions: equatorial

719 zone, subtropical region, mid-latitude region and Arctic. The average  
720 temperature profiles in these four regions are shown in Fig. 10. The  
721 retrieval temperature varies from place to place and changes with  
722 atmospheric conditions. In order to further compare the regional  
723 differences of inversion accuracy, the temperature standard  
724 deviations of ICS in four typical regions are compared in Sect. 5.2.  
725



726

727 **Figure 10.** The average temperature profiles in four typical regions.  
728 Red line indicates the equatorial zone. Pink dotted line stands for the  
729 subtropics. Blue dotted line represents the mid-latitude region. Black  
730 dotted line stands for the Arctic.

731



732

### 733 **5.1 Experimental scheme**

734 In order to further illustrate the different accuracy of the retrieval  
735 temperature using our improved channel selection method under  
736 different atmospheric conditions, the profiles in four typical regions  
737 were used for statistical inversion comparison experiments. The  
738 experimental steps are as follows:

739 (1) 2500 profiles in Sect. 4 are used to work out the regression  
740 coefficient.

741 (2) The atmospheric profiles of the four typical regions: equatorial  
742 zone, subtropical region, mid-latitude region and Arctic are used for  
743 statistical inversion comparison experiments and test the result.(3)  
744 Verification of the results. The test is carried out based on the  
745 standard deviation between the retrieval value and the true value.

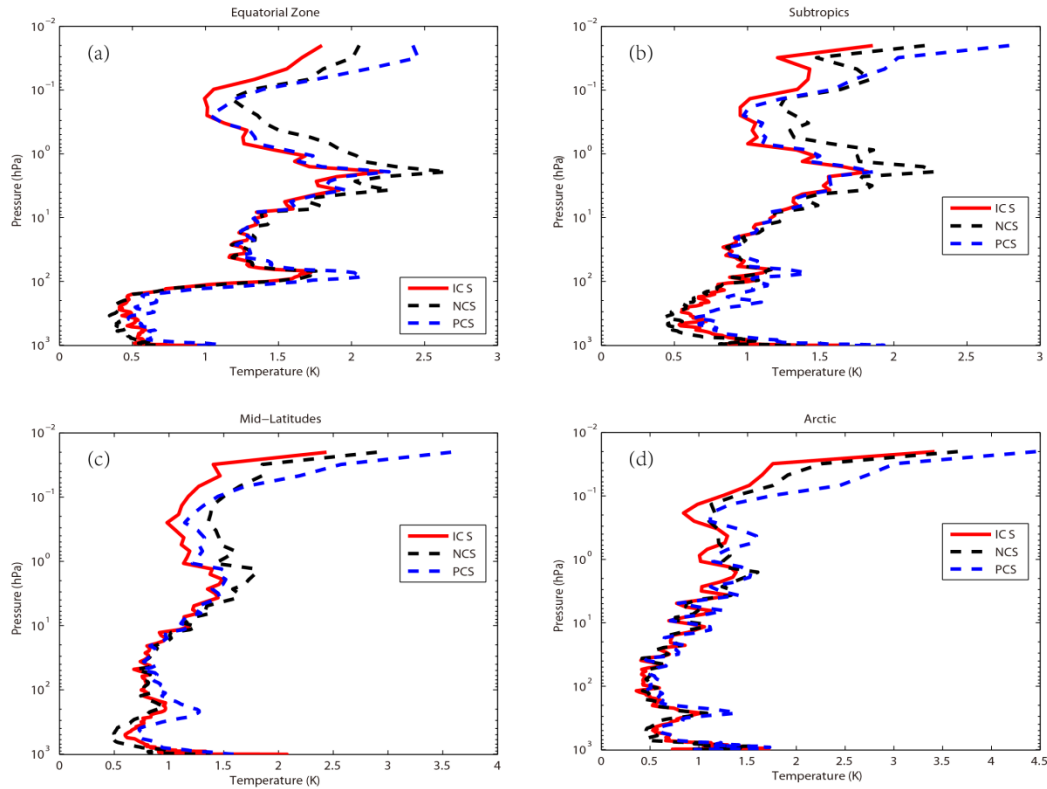
746

### 747 **5.2 Results and Discussion**

748 Using statistical inversion comparison experiments in four typical  
749 regions, the standard deviation of temperature retrieval is shown in  
750 Fig. 11. Generally, the retrieval temperature by ICS is better than  
751 that of NCS and PCS. In particular, above 1 hPa (the stratosphere  
752 and mesosphere), the standard deviation of atmospheric temperature  
753 can be improved by 1 K with PCS and NCS. Thus, ICS shows a

754 great improvement. The results were consistent with Sect. 4.

755



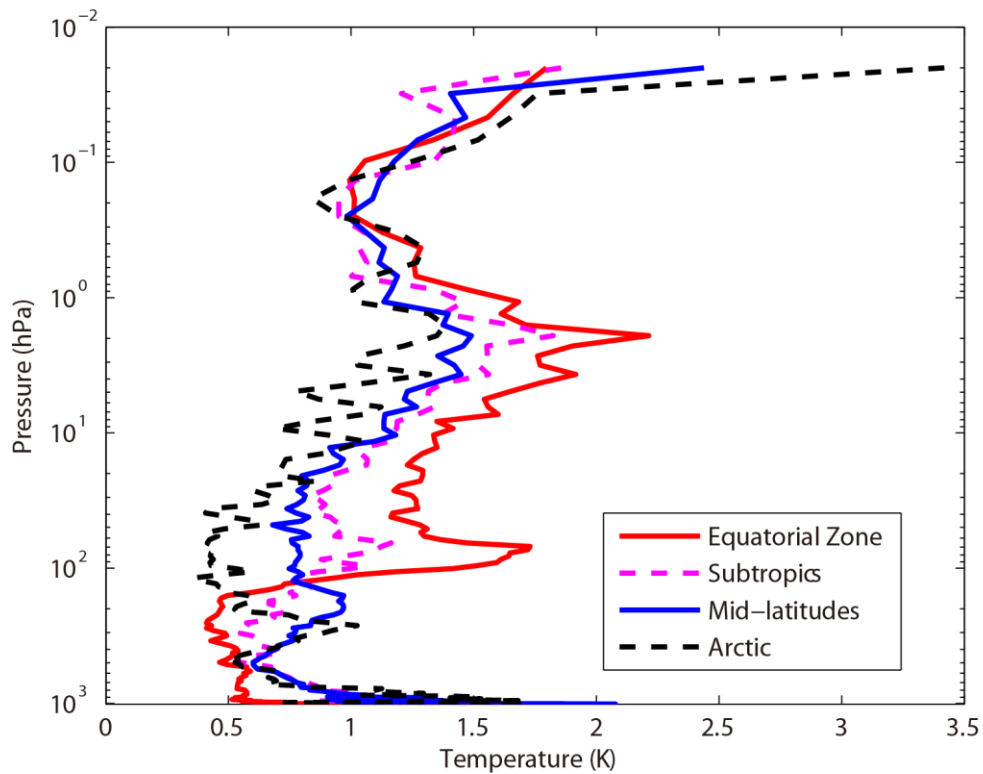
756

757 **Figure 11.** The temperature profile standard deviation of statistical  
758 inversion comparison experiments in four typical regions. Red line  
759 indicates the result of ICS. Black dotted line stands for the result of  
760 NCS. Blue dotted line represents the result of PCS. (a) Equatorial  
761 zone. (b) Subtropics. (c) Mid-latitudes. (d) Arctic.

762

763 In order to further compare the regional differences of inversion  
764 accuracy, the temperature standard deviation of ICS in four typical  
765 regions are compared in Fig. 12.

766



767

768 **Figure 12.** The temperature standard deviation of ICS in four typical  
 769 regions. Red line indicates the result of equatorial zone. Pink dotted  
 770 line represents the result of Subtropics. Blue line represents the  
 771 result of Mid-latitudes. Black dotted line stands for the result of  
 772 Arctic.

773

774 The temperature standard deviations of the ICS in the four typical  
 775 regions are large (Fig. 12). Below 100 hPa, due to the high  
 776 temperature in the equatorial zone, the channel combination of ICS  
 777 is better than that of PCS and NCS for atmospheric temperature  
 778 observation to the higher temperature. The standard deviation is  
 779 0.5K. Due to the method selected in this paper there are more

780 channels at 4.2  $\mu\text{m}$  for  $\text{N}_2\text{O}$  and 4.3  $\mu\text{m}$  for  $\text{CO}_2$  absorption bands  
781 which has been previously described in Sect. 3. Near the tropopause,  
782 the standard deviation of the equatorial zone increases sharply. It is  
783 also due to the sharp drops in temperature. However, the standard  
784 deviation of the Arctic is still around 0.5K. From 100hPa to 1hPa,  
785 the standard deviation of ICS is 0.5 K to 2K. With the increase of  
786 latitude, the effectiveness considerably increases. According to Fig.  
787 11, ICS takes channel sensitivity as a function of height into  
788 consideration, so its retrieval result is better.

789 Although the improvements of ICS in the four typical regions are  
790 different, in general, the accuracy of the retrieval temperature of ICS  
791 is improved. Because PCS does not take channel sensitivity as a  
792 function of height into consideration, the retrieval result of PCS is  
793 inferior to that of ICS. In general, the accuracy of the retrieval  
794 temperature of ICS is improved.

795

## 796 **7 Conclusions**

797 In recent years, the atmospheric layer in the altitude range of about  
798 20–100 km has been named “the near space layer” by aeronautical  
799 and astronautical communities. It is between the space-based  
800 satellite platform and the aerospace vehicle platform, which is the  
801 transition zone between aviation and aerospace. Its unique resource

802 has attracted a lot of attention from many countries. Research and  
803 exploration, therefore, on and of the near space layer are of great  
804 importance. A new channel selection scheme and method for  
805 hyperspectral atmospheric infrared sounder AIRS data based on  
806 layering is proposed. The retrieval results of ICS concerning the near  
807 space atmosphere are particularly good. Thus, ICS aims to provide a  
808 new and an effective channel selection method for the study of the  
809 near space atmosphere using the hyperspectral atmospheric infrared  
810 sounder.

811 An improved channel selection method is proposed, based on  
812 information content in this paper. A robust channel selection scheme  
813 and method are proposed, and a series of channel selection  
814 comparison experiments are conducted. The results are as follows:

815 (1) Since ICS takes channel sensitivity as a function of height into  
816 consideration, the ARI of PCS only tends to be 0.38 and is not  
817 convergent. However, as the 100<sup>th</sup> iteration is approached, the ARI of  
818 ICS tends to be stable, reaching 0.54, while the distribution of the  
819 temperature weighting function is more continuous and closer to that  
820 of the actual atmosphere. Thus, in terms of the ARI, convergence,  
821 and the distribution of the temperature weighting function, ICS is  
822 better than PCS.

823 (2) Statistical inversion comparison experiments show that the

824 retrieval temperature of ICS in this paper is consistent with that of  
825 NCS. In particular, from 10 hPa to 0.02 hPa (the stratosphere and  
826 mesosphere), the retrieval temperature of ICS is obviously better  
827 than that of NCS at about 1 K. In general, the accuracy of the  
828 retrieval temperature of ICS is improved. Especially, from 100 hPa  
829 to 0.01 hPa, the accuracy of ICS can be improved by more than 11%.  
830 The reason is that stratosphere and mesosphere are less affected by  
831 the ground surface, so the retrieval result of ICS is better than that of  
832 NCS. Additionally, due to the method selected in this paper there are  
833 more channels at 4.2  $\mu\text{m}$  for the  $\text{N}_2\text{O}$  and at 4.3  $\mu\text{m}$  for the  $\text{CO}_2$   
834 absorption bands; the channel combination of ICS is better than that  
835 of NCS for atmospheric temperature observation to the higher  
836 temperature.

837 (3) Statistical inversion comparison experiments in four typical  
838 regions indicate that ICS in this paper is significantly better than  
839 NCS and PCS in different regions and shows latitudinal variations,  
840 which shows potential for future applications.

841

842 *Data availability.* The data used in this paper are available from the  
843 corresponding author upon request.

844

845 *Appendices*

846 Appendix A

847 **Table A1.** Pressure levels adopted for RTTOV v12 54 pressure level  
 848 coefficients and profile limits within which the transmittance  
 849 calculations are valid. Note that the gas units here are ppmv.  
 850 (From <https://www.nwpsaf.eu/site/software/rttov/>, RTTOV Users  
 851 guide, 2019).

Level	Pressure	Tmax	Tmin	Qmax	Qmin	Q <sub>2</sub> max	Q <sub>2</sub> min	Q <sub>2</sub> Ref
Number	hPa	K	K	ppmv*	ppmv*	ppmv*	ppmv*	ppmv*
1	0.01	245.95	143.66	5.24	0.91	1.404	0.014	0.296
2	0.01	252.13	154.19	6.03	1.08	1.410	0.069	0.321
3	0.03	263.71	168.42	7.42	1.35	1.496	0.108	0.361
4	0.03	280.12	180.18	8.10	1.58	1.670	0.171	0.527
5	0.13	299.05	194.48	8.44	1.80	2.064	0.228	0.769
6	0.23	318.64	206.21	8.59	1.99	2.365	0.355	1.074
7	0.41	336.24	205.66	8.58	2.49	2.718	0.553	1.471
8	0.67	342.08	197.17	8.34	3.01	3.565	0.731	1.991
9	1.08	340.84	189.50	8.07	3.30	5.333	0.716	2.787
10	1.67	334.68	179.27	7.89	3.20	7.314	0.643	3.756
11	2.50	322.5	176.27	7.75	2.92	9.191	0.504	4.864
12	3.65	312.51	175.04	7.69	2.83	10.447	0.745	5.953
13	5.19	303.89	173.07	7.58	2.70	12.336	1.586	6.763
14	7.22	295.48	168.38	7.53	2.54	12.936	1.879	7.109
15	9.84	293.33	166.30	7.36	2.46	12.744	1.322	7.060
16	13.17	287.05	163.47	7.20	2.42	11.960	0.719	6.574
17	17.33	283.36	161.49	6.96	2.20	11.105	0.428	5.687
18	22.46	280.93	161.47	6.75	1.71	9.796	0.278	4.705
19	28.69	282.67	162.09	6.46	1.52	8.736	0.164	3.870
20	36.17	279.93	162.49	6.14	1.31	7.374	0.107	3.111

21	45.04	27315	164.66	5.90	1.36	6.799	0.055	2.478
22	55.44	265.93	166.19	6.21	1.30	5.710	0.048	1.907
23	67.51	264.7	167.42	9.17	1.16	4.786	0.043	1.440
24	81.37	261.95	159.98	17.89	0.36	4.390	0.038	1.020
25	97.15	262.43	163.95	20.30	0.01	3.619	0.016	0.733
26	114.94	259.57	168.59	33.56	0.01	2.977	0.016	0.604
27	134.83	259.26	169.71	102.24	0.01	2.665	0.016	0.489
28	156.88	260.13	169.42	285.00	0.01	2.351	0.013	0.388
29	181.14	262.27	17063	714.60	0.01	1.973	0.010	0.284
30	207.61	264.45	174.11	1464.00	0.01	1.481	0.013	0.196
31	236.28	270.09	177.12	2475.60	0.01	1.075	0.016	0.145
32	267.10	277.93	181.98	4381.20	0.01	0.774	0.015	0.110
33	300.00	285.18	184.76	6631.20	0.01	0.628	0.015	0.086
34	334.86	293.68	187.69	9450.00	1.29	0.550	0.016	0.073
35	371.55	300.12	190.34	12432.00	1.52	0.447	0.015	0.063
36	409.89	302.63	194.40	15468.00	2.12	0.361	0.015	0.057
37	449.67	304.43	198.46	18564.00	2.36	0.284	0.015	0.054
38	490.&5	307.2	201.53	21684.00	2.91	0.247	0.015	0.052
39	532.56	31217	202.74	24696.00	3.67	0.199	0.015	0.050
40	572.15	31556	201.61	27480.00	3.81	0.191	0.012	0.050
41	618.07	318.26	189.95	30288.00	6.82	0.171	0.010	0.049
42	661.00	321.71	189.95	32796.00	6.07	0.128	0.009	0.048
43	703.59	327.95	189.95	55328.00	6.73	0.124	0.009	0.047
44	745.48	333.77	189.95	37692.00	8.71	0.117	0.009	0.046
45	786.33	336.46	189.95	39984.00	8.26	0.115	0.008	0.045
46	825.75	338.54	189.95	42192.00	7.87	0.113	0.008	0.043
47	863.40	342.55	189.95	44220.00	7.53	0.111	0.007	0.041
48	898.93	346.23	189.95	46272.00	7.23	0.108	0.006	0.040
49	931.99	34924	189.95	47736.00	6.97	0.102	0.006	0.038
50	962.26	349.92	189.95	51264.00	6.75	0.099	0.006	0.034



51	989.45	350.09	189.95	49716.00	6.57	0.099	0.006	0.030
52	1013.29	360.09	189.95	47208.00	6.41	0.094	0.006	0.028
53	1033.54	350.09	189.95	47806.00	6.29	0.094	0.006	0.027
54	1050.00	350.09	189.95	47640.00	6.19	0.094	0.006	0.027

852

853 **Table A2.** Pressure levels adopted for IFS-137 137 pressure levels

854 (in hPa).

Level number	pressure hPa	Level number	pressure hPa	Level number	pressure hPa	Level number	pressure hPa	Level number	pressure hPa
1	0.02	31	12.8561	61	106.4153	91	424.019	121	934.7666
2	0.031	32	14.2377	62	112.0681	92	441.5395	122	943.1399
3	0.0467	33	15.7162	63	117.9714	93	459.6321	123	950.9082
4	0.0683	34	17.2945	64	124.1337	94	478.3096	124	958.1037
5	0.0975	35	18.9752	65	130.5637	95	497.5845	125	964.7584
6	0.1361	36	20.761	66	137.2703	96	517.4198	126	970.9046
7	0.1861	37	22.6543	67	144.2624	97	537.7195	127	976.5737
8	0.2499	38	24.6577	68	151.5493	98	558.343	128	981.7968
9	0.3299	39	26.7735	69	159.1403	99	579.1926	129	986.6036
10	0.4288	40	29.0039	70	167.045	100	600.1668	130	991.023
11	0.5496	41	31.3512	71	175.2731	101	621.1624	131	995.0824
12	0.6952	42	33.8174	72	183.8344	102	642.0764	132	998.8081
13	0.869	43	36.4047	73	192.7389	103	662.8084	133	1002.225
14	1.0742	44	39.1149	74	201.9969	104	683.262	134	1005.356
15	1.3143	45	41.9493	75	211.6186	105	703.3467	135	1008.224
16	1.5928	46	44.9082	76	221.6146	106	722.9795	136	1010.849
17	1.9134	47	47.9915	77	231.9954	107	742.0855	137	1013.25
18	2.2797	48	51.199	78	242.7719	108	760.5996		
19	2.6954	49	54.5299	79	253.9549	109	778.4661		
20	3.1642	50	57.9834	80	265.5556	110	795.6396		
21	3.6898	51	61.5607	81	277.5852	111	812.0847		
22	4.2759	52	65.2695	82	290.0548	112	827.7756		
23	4.9262	53	69.1187	83	302.9762	113	842.6959		
24	5.6441	54	73.1187	84	316.3607	114	856.8376		
25	6.4334	55	77.281	85	330.2202	115	870.2004		
26	7.2974	56	81.6182	86	344.5663	116	882.791		
27	8.2397	57	86.145	87	359.4111	117	894.6222		
28	9.2634	58	90.8774	88	374.7666	118	905.7116		
29	10.372	59	95.828	89	390.645	119	916.0815		

855 *Author contributions.* ZS contributed the central idea. SC, ZS and  
856 HD conceived the method, developed the retrieval algorithm and  
857 discussed the results. SC analyzed the data, prepared the figures and  
858 wrote the paper. WG contributed to refining the ideas, carrying out  
859 additional analyses. All co-authors reviewed the paper.

860

861 *Competing interests.* The authors declare that they have no conflict  
862 of interest.

863

864 *Acknowledgements.* The study was supported by the National Key  
865 Research Program of China: Development of high-resolution data  
866 assimilation technology and atmospheric reanalysis data set in East  
867 Asia (Research on remote sensing telemetry data assimilation  
868 technology, Grant no. 2017YFC1501802). The study was also  
869 supported by the National Natural Science Foundation of China  
870 (Grant no. 41875045) and Hunan Provincial Innovation Foundation  
871 for Postgraduate (Grant no. CX2018B033 and no. CX2018B034).

872

## 873 **References**

874 Aires, F., Schmitt, M., Chedin, A., and Scott, N.: The “weighting  
875 smoothing” regularization of MLP for Jacobian stabilization,

876 IEEE. T. Neural. Networks., 10, 1502-1510,  
877 <https://doi.org/10.1109/72.809096>, 1999.

878 Aires, F., Chédin, Alain., Scott, N. A., and Rossow, W. B.: A  
879 regularized neural net approach for retrieval of atmospheric and  
880 surface temperatures with the IASI instrument, J. Appl. Meteorol.,  
881 41,144-159,  
882 [https://doi.org/10.1175/1520-0450\(2002\)041<0144:ARNNAF>2.0](https://doi.org/10.1175/1520-0450(2002)041<0144:ARNNAF>2.0)  
883 .CO;2, 2002.

884 Aumann, H. H.: Atmospheric infrared sounder on the earth  
885 observing system, Optl. Engr., 33, 776-784,  
886 <https://doi.org/10.1117/12.159325>, 1994.

887 Aumann, H. H., Chahine, M. T., Gautier, C., and Goldberg, M.:  
888 AIRS/AMSU/HSB on the Aqua mission: design, science objective,  
889 data products, and processing systems, IEEE. Trans. GRS.,  
890 41,253-264, <http://dx.doi.org/10.1109/TGRS.2002.808356>, 2003.

891 Brath, M., Fox, S., Eriksson, P., Harlow, R. C., Burgdorf, M., and  
892 Buehler, S. A.: Retrieval of an ice water path over the ocean from  
893 ISMAR and MARSS millimeter and submillimeter brightness  
894 temperatures, Atmos. Meas. Tech., 11, 611–632,  
895 <https://doi.org/10.5194/amt-11-611-2018>, 2018.

896 Chahine, M. I.: A general relaxation method for inverse solution of  
897 the full radiative transfer equation, J. Atmos. Sci., 29, 741-747,

898 [https://doi.org/10.1175/1520-0469\(1972\)029<0741:AGRMFI>2.0](https://doi.org/10.1175/1520-0469(1972)029<0741:AGRMFI>2.0)  
899 CO;2, 1972.

900 Chang, K. W, L'Ecuyer, T. S., Kahn, B. H., and Natraj, V.:  
901 Information content of visible and midinfrared radiances for  
902 retrieving tropical ice cloud properties, *J. Geophys. Res.*, 122,  
903 <https://doi.org/10.1002/2016JD026357>, 2017.

904 Chedin, A., Scott, N. A., Wahiche, C., and Moulinier, P.: The  
905 improved initialization inversion method: a high resolution  
906 physical method for temperature retrievals from satellites of the  
907 tiros-n series, *J. Appl. Meteor.*, 24, 128-143,  
908 [https://doi.org/10.1175/1520-0450\(1985\)024<0128:TIHIMA>2.0.C](https://doi.org/10.1175/1520-0450(1985)024<0128:TIHIMA>2.0.C)  
909 O;2, 1985.

910 Cyril, C., Alain, C., and Scott, N. A.: Airs channel selection for CO<sub>2</sub>  
911 and other trace-gas retrievals, *Q. J. Roy. Meteor. Soc.*, 129,  
912 2719-2740, <https://doi.org/10.1256/qj.02.180>, 2003.

913 Du, H. D., Huang, S. X., and Shi, H. Q.: Method and experiment of  
914 channel selection for high spectral resolution data, *Acta. Physica.*  
915 *Sinica.*, 57, 7685-7692, 2008 .

916 Dudhia, A., Jay, V. L., and Rodgers, C. D.: Microwindow selection  
917 for high-spectral-resolution sounders, *Appl. Opt.* 41, 3665-3673,  
918 <https://doi.org/10.1364/AO.41.003665>, 2002.

919 Eresmaa, R. and McNally, A. P.: Diverse profile datasets from the

920 ECMWF 137-level short-range forecasts, Tech. rep., ECMWF,  
921 2014.

922 Eyre, J. R., Andersson E., and McNally, A. P.: Direct use of  
923 satellite sounding radiances in numerical weather prediction, High  
924 Spectral Resolution Infrared Remote Sensing for Earth's Weather  
925 and Climate Studies, Springer, Berlin, Heidelberg,  
926 [https://doi.org/10.1007/978-3-642-84599-4\\_25](https://doi.org/10.1007/978-3-642-84599-4_25), 1993.

927 Fang, Z. Y.: The evolution of meteorological satellites and the  
928 insight from it, *Adv. Meteorol. Sci. Technol.*, 4, 27-34,  
929 <https://doi.org/10.3969/j.issn.2095-1973.2014.06.003>, 2014.

930 Gong, J., Wu, D. L., and Eckermann, S. D.: Gravity wave variances  
931 and propagation derived from AIRS radiances, *Atmos. Chem.*  
932 *Phys.*, 11, 11691-11738,  
933 <https://doi.org/10.5194/acp-12-1701-2012>, 2011.

934 He, M. Y., Du, H. D., Long, Z. Y., and Huang, S. X.: Selection of  
935 regularization parameters using an atmospheric retrievable index  
936 in a retrieval of atmospheric profile, *Acta. Physica Sinica.*, 61,  
937 024205-160, 2012.

938 Hoffmann, L. and Alexander, M. J.: Retrieval of stratospheric  
939 temperatures from atmospheric infrared sounder radiance  
940 measurements for gravity wave studies, *J. Geophys. Res. Atm.*,  
941 114, <https://doi.org/10.1029/2008JD011241>, 2009.

942 Huang, H. L., Li, J., Baggett, K., Smith, W. L., and Guan, L.:  
943 Evaluation of cloud-cleared radiances for numerical weather  
944 prediction and cloud-contaminated sounding applications,  
945 Atmospheric and Environmental Remote Sensing Data Processing  
946 and Utilization: Numerical Atmospheric Prediction and  
947 Environmental Monitoring, I. S. O. Photonics.,  
948 <https://doi.org/10.1117/12.613027>, 2005.

949 Kuai, L., Natraj, V., Shia, R. L., Miller, C., and Yung, Y. L.: Channel  
950 selection using information content analysis: a case study of CO<sub>2</sub>  
951 retrieval from near infrared measurements. J. Q. S. Radiative.  
952 Transfer., 111, 1296-1304,  
953 <https://doi.org/10.1016/j.jqsrt.2010.02.011>, 2010.

954 Li, J., Wolf, W. W., Menzel, W. P., Paul, Menzel. W., Zhang, W. J.,  
955 Huang, H. L., and Achtor, T. H.: Global soundings of the  
956 atmosphere from ATOVS measurements: the algorithm and  
957 validation, J. Appl. Meteor., 39, 1248-1268,  
958 [https://doi.org/10.1175/1520-0450\(2000\)039<1248:GSOTAF>2.0](https://doi.org/10.1175/1520-0450(2000)039<1248:GSOTAF>2.0).  
959 CO;2, 2000.

960 Li, J., Liu, C. Y., Huang, H. L., Schmit, T. J., Wu, X., Menzel, W. P.,  
961 and Gurka, J. J.: Optimal cloud-clearing for AIRS radiances using  
962 MODIS, IEEE. Trans. GRS. , 43, 1266-1278, [http://dx.doi.org/](http://dx.doi.org/10.1109/tgrs.2005.847795)  
963 [10.1109/tgrs.2005.847795](http://dx.doi.org/10.1109/tgrs.2005.847795), 2005.

964 Liu, Z. Q.: A regional ATOVS radiance-bias correction scheme for  
965 radiance assimilation, *Acta. Meteorologica. Sinica.*, 65, 113-123,  
966 2007.

967 Lupu, C., Gauthier, P., and Laroche, Stéphane.: Assessment of the  
968 impact of observations on analyses derived from observing system  
969 experiments, *Mon. Weather. Rev.*, 140, 245-257,  
970 <https://doi.org/10.1175/MWR-D-10-05010.1>, 2012.

971 Menke, W.: *Geophysical Data Analysis: Discrete Inverse Theory*,  
972 Acad. Press., Columbia University, New York,  
973 <https://doi.org/10.1016/B978-0-12-397160-9.00019-9>, 1984.

974 Menzel, W. P., Schmit, T. J., Zhang, P. and Li, J.: Satellite-based  
975 atmospheric infrared sounder development and applications, *Bull.*  
976 *Amer. Meteor. Soc.*, 99, 583–603,  
977 <https://doi.org/10.1175/BAMS-D-16-0293.1>, 2018.

978 Prunet, P., Thépaut J. N., and Cass, V.: The information content of  
979 clear sky IASI radiances and their potential for numerical weather  
980 prediction, *Q. J. Roy. Meteor. Soc.*, 124, 211-241,  
981 <https://doi.org/10.1002/qj.49712454510>, 2010.

982 Xu, Q.: Measuring information content from observations for data  
983 assimilation: relative entropy versus shannon entropy difference,  
984 *Tellus. A.*, 59, 198-209,  
985 <https://doi.org/10.1111/j.1600-0870.2006.00222.x>, 2007.

986 Rabier, F., Fourrié, N., and Chafâi, D.: Channel selection methods  
987 for infrared atmospheric sounding interferometer radiances, Q. J.  
988 Roy. Meteor. Soc., 128, 1011-1027,  
989 <https://doi.org/10.1256/0035900021643638>, 2010.

990 Richardson, M. and Stephens, G. L.: Information content of oco-2  
991 oxygen a-band channels for retrieving marine liquid cloud  
992 properties, Atmospheric Measurement Techniques, 11, 1-19,  
993 <https://doi.org/10.5194/amt-11-1515-2018>, 2018.

994 Rodgers, C. D.: Information content and optimisation of high  
995 spectral resolution remote measurements, Adv. Spa. Research, 21,  
996 136-147, [https://doi.org/10.1016/S0273-1177\(97\)00915-0](https://doi.org/10.1016/S0273-1177(97)00915-0), 1996.

997 Rodgers, C. D.: Inverse Methods for Atmospheric Sounding, Inverse  
998 methods for atmospheric sounding, World Scientific,  
999 <https://doi.org/10.1142/3171>, 2000.

1000 Saunders, R., Hocking, J., Turner, E., Rayer, P., Rundle, D., Brunel,  
1001 P., Vidot, J., Roquet, P., Matricardi, M., Geer, A., Bormann, N.,  
1002 and Lupu, C.: An update on the RTTOV fast radiative transfer  
1003 model (currently at version 12), Geosci. Model Dev., 11,  
1004 2717-2737, <https://doi.org/10.5194/gmd-11-2717-2018>, 2018.

1005 Susskind, J., Barnett, C. D. and Blaisdell, J. M.: Retrieval of  
1006 atmospheric and surface parameters from AIRS/AMSU/HSB data  
1007 in the presence of clouds, IEEE Trans. Geosci. Remote Sensing,



1008 41, 390-409, <https://doi.org/10.1109/TGRS.2002.808236>, 2003.

1009 Smith, W. L., Woolf, H. M., and Revercomb, H. E.: Linear  
1010 simultaneous solution for temperature and absorbing constituent  
1011 profiles from radiance spectra, *Appl. Optics.*, 30, 1117,  
1012 <https://doi.org/10.1364/AO.30.001117>, 1991.

1013 Wakita, H., Tokura, Y., Furukawa, F., and Takigawa, M.: Study of  
1014 the information content contained in remote sensing data of  
1015 atmosphere, *Acta. Physica. Sinica.*, 59, 683-691, 2010.

1016 Wang, G., Lu, Q. F., Zhang, J. W., and Wang, H. Y.,.: Study on  
1017 method and experiment of hyper-spectral atmospheric infrared  
1018 sounder channel selection, *Remote Sensing Technology and  
1019 Application.*, 29, 795-802 , 2014.

1020 Zhang, J. W., Wang, G., Zhang, H., Huang J., Chen J., and Wu, L. L.:  
1021 Experiment on hyper-spectral atmospheric infrared sounder  
1022 channel selection based on the cumulative effect coefficient of  
1023 principal component, *Journal of Nanjing Institute of meteorology*,  
1024 1, 36-42, <http://dx.doi.org/10.3969/j.issn.1674-7097.2011.01.005>,  
1025 2011.